

1 **Intercomparison of model simulations of mixed-phase**  
2 **clouds observed during the ARM Mixed-Phase Arctic**  
3 **Cloud Experiment. Part I: Single layer cloud**

4 Stephen A. Klein<sup>1</sup>, Renata B. McCoy<sup>1</sup>, Hugh Morrison<sup>2</sup>, Andrew S. Ackerman<sup>3</sup>,  
5 Alexander Avramov<sup>4</sup>, Gijs de Boer<sup>5</sup>, Mingxuan Chen<sup>6</sup>, Jason N. S. Cole<sup>7</sup>, Anthony D.  
6 Del Genio<sup>3</sup>, Michael Falk<sup>8</sup>, Michael J. Foster<sup>9</sup>, Ann Fridlind<sup>3</sup>, Jean-Christophe Golaz<sup>10</sup>,  
7 Tempei Hashino<sup>5</sup>, Jerry Y. Harrington<sup>4</sup>, Corinna Hoose<sup>11</sup>, Marat F. Khairoutdinov<sup>12</sup>,  
8 Vincent E. Larson<sup>8</sup>, Xiaohong Liu<sup>13</sup>, Yali Luo<sup>14</sup>, Greg M. McFarquhar<sup>15</sup>, Surabi Menon<sup>16</sup>,  
9 Roel A. J. Neggers<sup>17</sup>, Sungsu Park<sup>18</sup>, Michael R. Poellot<sup>19</sup>, Jerome M. Schmidt<sup>20</sup>, Igor  
10 Sednev<sup>16</sup>, Ben J. Shipway<sup>21</sup>, Matthew D. Shupe<sup>22</sup>, Douglas A. Spangenberg<sup>23</sup>, Yogesh C.  
11 Sud<sup>24</sup>, David D. Turner<sup>5</sup>, Dana E. Veron<sup>25</sup>, Knut von Salzen<sup>26</sup>, Gregory K. Walker<sup>27</sup>,  
12 Zhien Wang<sup>27</sup>, Audrey B. Wolf<sup>3</sup>, Shaocheng Xie<sup>1</sup>, Kuan-Man Xu<sup>28</sup>, Fanglin Yang<sup>29</sup>, and  
13 Gong Zhang<sup>15</sup>

14 <sup>1</sup>Lawrence Livermore National Laboratory, Livermore, CA, USA

15 <sup>2</sup>National Center for Atmospheric Research, Boulder, CO, USA

16 <sup>3</sup>NASA Goddard Institute for Space Studies, New York, NY, USA

17 <sup>4</sup>The Pennsylvania State University, University Park, PA, USA

18 <sup>5</sup>University of Wisconsin – Madison, Madison, WI, USA

19 <sup>6</sup>Colorado State University, Fort Collins, CO, USA

20 <sup>7</sup>University of British Columbia, Vancouver, BC, Canada

21 <sup>8</sup>University of Wisconsin – Milwaukee, Milwaukee, WI, USA

22 <sup>9</sup>Rutgers University, New Brunswick, NJ, USA

23 <sup>10</sup>NOAA Geophysical Fluid Dynamics Laboratory, Princeton, NJ, USA

24 <sup>11</sup>ETH Zurich, Institute for Atmospheric and Climate Science, Zurich, Switzerland

25 <sup>12</sup>State University of New York at Stony Brook, Stony Brook, NY, USA

26 <sup>13</sup>Pacific Northwest National Laboratory, Richland, WA, USA

27 <sup>14</sup>State Key Laboratory of Severe Weather, Chinese Academy of Meteorological Sciences, Beijing, China

28 <sup>15</sup>University of Illinois, Urbana, IL, USA

29 <sup>16</sup>Lawrence Berkeley National Laboratory, Berkeley, CA, USA

30 <sup>17</sup>KNMI, Utrecht, Netherlands

31 <sup>18</sup>University of Washington, Seattle, WA, USA

1 <sup>19</sup>University of North Dakota, Grand Forks, North Dakota, USA  
2 <sup>20</sup>Navy Research Laboratory, Monterey, CA, USA  
3 <sup>21</sup>Met Office, Exeter, United Kingdom  
4 <sup>22</sup>Cooperative Institute for Research in Environmental Sciences, University of Colorado / NOAA, Boulder,  
5 CO, USA  
6 <sup>23</sup>Science Systems and Applications, Inc., Hampton, VA, USA  
7 <sup>24</sup>NASA Goddard Space Flight Center, Greenbelt, MD, USA  
8 <sup>25</sup>University of Delaware, Newark, DE, USA  
9 <sup>26</sup>Canadian Center for Climate, Vancouver, British Columbia, Canada  
10 <sup>27</sup>University of Wyoming, Laramie, WY, USA  
11 <sup>28</sup>NASA Langley Research Center, Hampton, VA, USA  
12 <sup>29</sup>National Centers for Environmental Prediction, Camp Springs, MD, USA  
13  
14  
15 Submitted to *Quarterly Journal of the Royal Meteorological Society* March 5, 2008;  
16 Revised, ??? 2008; Accepted, xxx 200x

17 \*Correspondence to: S. Klein, PCMDI, Lawrence Livermore National Laboratory,  
18 Livermore, California, 94551, USA. E-mail: [klein21@llnl.gov](mailto:klein21@llnl.gov)

19

1 **Abstract**

2 Results are presented from an intercomparison of single-column and cloud-resolving  
3 model simulations of a cold-air outbreak mixed-phase stratocumulus cloud observed  
4 during the Atmospheric Radiation Measurement (ARM) program's Mixed-Phase Arctic  
5 Cloud Experiment. The observed cloud occurred in a well-mixed boundary layer with a  
6 cloud top temperature of  $-15^{\circ}\text{C}$ . The observed average liquid water path of around  $160\text{ g}$   
7  $\text{m}^{-2}$  was about two-thirds of the adiabatic value and much greater than the average mass  
8 of ice crystal precipitation which when integrated from the surface to cloud top was  
9 around  $15\text{ g m}^{-2}$ .

10 The simulations were performed by seventeen single-column models (SCMs) and nine  
11 cloud-resolving models (CRMs). While the simulated ice water path is generally  
12 consistent with the observed values, the median SCM and CRM liquid water path is a  
13 factor of three smaller than observed. Results from a sensitivity study in which models  
14 removed ice microphysics suggest that in many models the interaction between liquid and  
15 ice-phase microphysics is responsible for the large model underestimate of liquid water  
16 path.

17 Despite this general underestimate, the simulated liquid and ice water paths of several  
18 models are consistent with the observed values. Furthermore, there is evidence that  
19 models with more sophisticated microphysics simulate liquid and ice water paths that are  
20 in better agreement with the observed values, although considerable scatter is also

- 1 present. Although no single factor guarantees a good simulation, these results emphasize
- 2 the need for improvement in the model representation of mixed-phase microphysics.

## 1 **1. Introduction**

2 The treatment of clouds continues to be a highly challenging aspect of climate and  
3 weather modeling. The parameterization of Arctic clouds has been especially difficult,  
4 given the paucity of observations in the region (Curry et al. 1996). However, several field  
5 programs in recent years have begun to address this deficiency, including the 1994  
6 Beaufort and Arctic Storms Experiment (Curry et al. 1997), 1997-1998 Surface Heat  
7 Budget of the Arctic Ocean Experiment (SHEBA, Uttal et al. 2002), the 1998 First  
8 International Satellite Cloud Climatology Project Regional Experiment – Arctic Clouds  
9 Experiment (Curry et al. 2000), and the ongoing ARM program site operating near  
10 Barrow, Alaska (Ackerman and Stokes 2003).

11 A major finding from these experiments was the observed frequency and persistence of  
12 supercooled liquid water and mixed-phase stratiform clouds throughout the year (Curry et  
13 al. 2000, Pinto et al. 2001, Intrieri et al. 2002, Korolev et al. 2003, Shupe and Intrieri  
14 2004). In contrast to mid-latitude cloud systems, there is little temperature dependence  
15 for the amount of liquid versus ice in Arctic mixed-phase clouds (Curry et al. 2000,  
16 Korolev et al. 2003, McFarquhar and Cober 2004, Turner 2005). These clouds may  
17 contain one or more thin liquid layers embedded within a deep cloud that extends from  
18 near the surface into the middle and upper troposphere (Pinto 1998, Hobbs and Rangno  
19 1998, Shupe et al. 2006). Ice crystals fall from the liquid layers and may reach the ground  
20 in the form of light snow or snow showers. During SHEBA, slightly more than half of the  
21 mixed-phase clouds consisted of a single low-level liquid layer, while the rest contained  
22 multiple liquid layers in a deep cloud ice layer (Shupe et al. 2006).

1 The frequent occurrence of mixed-phase clouds has important implications for the cloud  
2 radiative forcing at the surface and the surface energy budget, since mixed-phase clouds  
3 tend to be optically thicker than ice-only clouds (Sun and Shine 1994, Shupe and Intrieri  
4 2004, Turner 2005, Zuidema et al. 2005). The presence of mixed-phase rather than ice-  
5 only clouds may also significantly impact the structure of the boundary layer and large-  
6 scale dynamics through the influence of cloud-top radiative cooling (Morrison and Pinto  
7 2006).

8 Climate and weather models tend to have difficulty predicting the observed frequency  
9 and persistence of Arctic mixed-phase clouds, leading to biases in surface radiative fluxes  
10 (Curry et al. 2000, Girard and Curry 2001, Morrison et al. 2003, Morrison and Pinto  
11 2006, Morrison et al. 2005b, Inoue et al. 2006, Prenni et al. 2007, Sandvik et al. 2007).  
12 These models tend to have difficulty simulating mid-latitude mixed-phase clouds as well  
13 (Illingworth et al. 2007). Studies have suggested that a more robust treatment of the  
14 modeled cloud microphysics is needed to improve simulations. Models with less  
15 sophisticated microphysics may incorrectly prescribe a ratio of liquid to ice mass that is  
16 inconsistent with Arctic observations. However, models with separate prognostic  
17 variables for liquid and ice and detailed microphysics may also produce poor simulations  
18 (Morrison et al. 2003, Inoue et al. 2006, Prenni et al. 2007, Sandvik et al. 2007). In these  
19 models, a more realistic treatment of ice microphysics, and in particular the number  
20 concentration of both small ice and snow, may be needed to improve results. Numerous  
21 modeling studies have demonstrated a strong sensitivity of mixed-phase clouds to ice  
22 number concentration (Pinto 1998, Harrington et al. 1999, Jiang et al. 2000, Morrison and

1 Pinto 2006, Prenni et al. 2007). Prenni et al. (2007) substantially improved their  
2 simulation of mixed-phase clouds by reducing ice nuclei number concentrations, which  
3 influence ice crystal number concentrations, from values typical of mid-latitudes to the  
4 low values observed in the Arctic. Their simulation was also sensitive to the  
5 representation of scavenging of ice nuclei by ice precipitation. Morrison and Pinto (2006)  
6 improved their simulation of Arctic mixed-phase stratus by reducing the specified  
7 intercept parameter of the snow size distribution; this is equivalent to reducing the snow  
8 number concentration for a given snow mixing ratio. These results increase the  
9 importance of resolving the long-standing uncertainty in the primary ice formation  
10 mechanisms in these clouds (Fridlind et al. 2007). Mixed-phase clouds may also be  
11 difficult to represent in large-scale models because their spatial scale may be smaller than  
12 the model grid spacing (Field et al. 2004). Several studies have suggested the role of  
13 small-scale (turbulent) updrafts in generating and maintaining regions of liquid water in  
14 these clouds (e.g., Mazin 1986; Korolev and Isaac 2003; Korolev and Field 2008).

15 To further our understanding of Arctic mixed-phase cloud processes and provide a  
16 detailed observational dataset for model evaluation, ARM conducted the Mixed-Phase  
17 Arctic Cloud Experiment (M-PACE, Verlinde et al. 2007) over northern Alaska and the  
18 adjacent Arctic Ocean during September and October 2004. During M-PACE, a suite of  
19 in-situ and remote sensors gathered measurements of mixed-phase cloud microphysics,  
20 dynamics, radiation, and aerosol. Already, several studies have used M-PACE  
21 observations to assess single-column, cloud-resolving, mesoscale, weather and climate  
22 model simulations of mixed-phase clouds (Xie et al. 2006, Fridlind et al. 2007, Liu et al.

1 2007b, Luo et al. 2008a, Luo et al. 2008b, Prenni et al. 2007, Morrison et al. 2008a, Xie  
2 et al. 2008, Sednev et al. 2008).

3 Given the impact of Arctic clouds on the surface radiation budget and the potential for  
4 significant climate feedbacks between sea-ice and clouds, it is vitally important that the  
5 representation of these clouds in weather-forecasting and climate models be improved.  
6 The Global Energy and Water Experiment Cloud Systems Study (GCSS) project (Randall  
7 et al. 2003) recognized this importance by devoting one of its working groups to the  
8 study of polar clouds. The GCSS project aims to improve the simulation of important  
9 cloud types in weather and climate models by bringing together the expertise of cloud-  
10 resolving modelers who understand the detailed cloud processes with that of large-scale  
11 modelers who develop parameterizations for these processes. A central activity of the  
12 GCSS project is the intercomparison study in which an observed case is simulated by  
13 CRMs and SCMs and model results compared to the observations. Indeed, new cloud  
14 parameterizations for both cloud-resolving and large-scale models are often first  
15 developed in and tested with simulations of GCSS intercomparison case studies.

16 This work presents the results of the first GCSS intercomparison case study of the Polar  
17 Cloud Working Group. This study involved simulations of mixed-phase clouds observed  
18 during two periods in M-PACE and was performed jointly with the ARM Cloud  
19 Modeling Working Group. The current paper, Part I, examines results for a single-layer  
20 mixed-phase stratocumulus cloud. The accompanying paper, Part II (Morrison et al.  
21 2008b), examines results for a deeper, multi-layered mixed-phase cloud. These two



1 periods were selected because single-layer mixed-phase boundary layer clouds and  
2 multi-layer mixed-phase clouds are two commonly occurring Arctic cloud types.  
3 Furthermore, the cloud processes for single and multi-layered clouds may be different.

4 The goal of this first intercomparison study is to document the current state of model  
5 simulations of Arctic mixed-phase clouds and to suggest future areas of work which the  
6 Polar Cloud Working Group may use to understand model differences and develop  
7 recommendations for parameterizations in large-scale models. This study presents the  
8 range of results and identifies common problems for the widest group of models possible,  
9 with the same initial and boundary conditions applied for each period to all simulations.

10 The wide range of participating models allows for a better generalization of results than  
11 was previously achieved in the model simulation studies cited above. Although it is not  
12 the goal of this study to completely understand model differences, a daunting task given  
13 the large number of models and their complexities, a few sensitivity studies are  
14 performed to gain some insight into these differences. Other GCSS intercomparison  
15 studies have been valuable in identifying important deficiencies in large-scale models  
16 such as an underestimate of the downdraft mass-fluxes associated with precipitating deep  
17 convection over land (Xie et al. 2002) and errors in the simulation of precipitation  
18 evaporation from drizzling marine stratocumulus clouds (Wyant et al. 2007).

19 The next section describes the synoptic situation for the single-layer mixed-phase  
20 stratocumulus that is the subject of this paper. Section 3 describes the cloud property  
21 observations from the in-situ and ground-based remote sensors that are used to assess

1 model simulations. Section 4 details the case specifications while Section 5 describes  
2 the seventeen SCMs and nine CRMs that participated in the intercomparison. Section 6  
3 compares model simulations to the available observations and Section 7 describes the  
4 result of two sensitivity studies. Section 8 briefly summarizes the key findings.

## 5 **2. Synoptic situation**

6 The boundary layer cloud system that is the focus of this study occurred during a period  
7 of northeasterly flow around an anticyclone to the north of Alaska (Verlinde et al. 2007).  
8 As the cold air above the sea ice to the northeast of Alaska flowed over the ice-free ocean  
9 adjacent to the coast, significant surface heat fluxes of temperature and water vapor  
10 induced the formation of boundary layer clouds in the form of “rolls” or “cloud-streets”  
11 which are common in “cold-air outbreak” stratocumulus (Figure 1). With the surface  
12 forcing, the boundary layer, as observed at the Alaska coast, was “well-mixed”. This was  
13 demonstrated by the fact that the vertical profiles of water vapor and potential  
14 temperature match those in which the variables of water and energy that are conserved  
15 during the condensation process are uniform in the boundary layer (Figure 2).

16 During the period of focus for this study, 17Z 9 October to 5Z 10 October 2004, the  
17 boundary layer was between 1000 and 1500 m deep at the coast of Alaska. As observed  
18 by both aircraft and ground-based remote sensors, the upper half of the boundary layer  
19 contained a mixed-phase cloud with a cloud top temperature of about  
20  $-15^{\circ}\text{C}$ . This cloud contained an amount of liquid water which in terms of condensate  
21 mass far exceeded the amount of ice present in the cloud. Beneath the cloud base, which

1 is identified here as the lowest level to contain liquid water, ice crystal precipitation  
2 occurred that reached the surface. The boundary layer was capped by a weak inversion of  
3 about 2K with dry and cloudless skies above.

### 4 **3. Cloud observations**

#### 5 a. Aircraft observations

6 During this period, there were two flights of the University of North Dakota Citation  
7 (McFarquhar et al. 2007b). The Citation performed a number of spirals above Barrow  
8 and Oliktok Point as well as ramped ascents or descents along the coastline between the  
9 two stations. From the two flights, there are a total of thirty-two vertical profiles which  
10 are analyzed in this study.

11 On board were probes that nominally measured the size distribution of particles with  
12 diameters between 3  $\mu\text{m}$  and 40  $\mu\text{m}$ , as well as the total condensate and liquid water  
13 contents separately. Interpretation of data from these probes is non-trivial and subject to  
14 uncertainties. Information on the phase, size distribution, and bulk microphysical  
15 parameters are from the analysis of McFarquhar et al. (2007b) who describe a  
16 methodology for intercomparison and interpretation of the aircraft data. Cloud phase was  
17 determined to be either liquid only, ice only, or mixed-phase from an algorithm that  
18 considered the output of an icing detector, visual inspection of particle images, and the  
19 shape of the particle size distribution. The phase classification was made for each 30 sec

1 flight segment that was determined to contain cloud (Figure 2 of McFarquhar et al.  
2 2007b). A 30 sec segment corresponds approximately to 2500 m of horizontal distance.

3 In addition to cloud phase, calculated bulk parameters include liquid and ice water  
4 contents as well as the particle number concentration and effective radius determined  
5 separately for liquid and ice in each 30 sec segment. Ice parameters correspond only to  
6 particles with diameters greater than 53  $\mu\text{m}$  because the characteristics of smaller ice  
7 crystals contain very large measurement uncertainties due to potential shattering of large  
8 ice crystals on the inlets and protruding shrouds of probes used to measure small ice  
9 crystals (McFarquhar et al. 2007a). Particles smaller than 0.125 mm measured by the  
10 two-dimensional cloud probe are not used because previous studies have suggested that  
11 there are problems with quantifying concentrations in this size range (Baumgardner and  
12 Korolev 1997, Strapp et al. 2001). The one-dimensional cloud probe is used, albeit with  
13 large uncertainty, to provide the concentration of particles between 0.05 and 0.125 mm.  
14 The liquid effective radius is calculated as the ratio of the third moment to the second  
15 moment of the liquid droplet size distribution. The effective radius of ice,  $r_i^{eff}$ , is  
16 calculated using the definition of Fu (1996) as  $r_i^{eff} = \sqrt{3IWC/3\rho_i A_c}$ , where  $IWC$  is the  
17 ice water content,  $\rho_i$  is a bulk ice density assumed to be  $910 \text{ kg m}^{-3}$ , and  $A_c$  is the  
18 projected cross-sectional area of ice crystals.

19 McFarquhar et al. (2007b) describe the uncertainties in the derived bulk parameters.  
20 Because the mixed-phase clouds are dominated by contributions of supercooled water,  
21 rough estimates of uncertainty are  $\pm 15\%$  for the bulk liquid parameters due to the

1 uncertainties in the King probe. There is a factor of two uncertainty for the bulk ice  
2 parameters, mainly due to uncertainties in the mass-diameter relation used for ice  
3 particles. The minimum detectable water content is on the order of  $0.001 \text{ g m}^{-3}$ .

#### 4 b. Ground-based remote sensor observations

5 Cloud physical and dynamical properties and surface radiative fluxes have been retrieved  
6 from the active and passive sensors deployed at Barrow and Oliktok Point. Two sets of  
7 mixed-phase cloud retrievals are available (Turner 2005, Shupe et al. 2006, Shupe 2007,  
8 Turner et al. 2007, Shupe et al. 2008, hereafter termed SHUPE-TURNER; Wang and Sassen  
9 2002, Wang 2007, hereafter termed WANG). The retrievals primarily rely on  
10 measurements from the millimeter wavelength cloud radar, lidar, and microwave  
11 radiometer. Except for liquid water path, cloud property retrievals are available only at  
12 Barrow.

13 Retrieved cloud physical properties include cloud top and base, cloud phase, the vertical  
14 profiles and vertically integrated amounts of liquid and ice water content, and the  
15 effective particle sizes of liquid and ice. Using a multi-sensor approach, Shupe (2007)  
16 derive a cloud phase mask that distinguishes target volumes into ice, liquid, mixed-phase,  
17 or clear categories. Although vertical profiles of liquid water content can be derived by  
18 scaling an assumed adiabatic liquid water profile to the observed liquid water path, in this  
19 study models are compared only to the microwave radiometer liquid water path of which  
20 two estimates are available (Turner et al. 2007, hereafter termed TURNER; WANG). Cloud  
21 ice properties are derived from seasonally-tuned radar retrievals (Shupe et al. 2006) or

1 from a combined radar-lidar method (Wang and Sassen 2002). For this case study,  
 2 rough uncertainty estimates are  $20 \text{ g m}^{-2}$  for the liquid water path (TURNER) and a factor  
 3 of two for the ice water content and path (Shupe et al. 2006). Based upon the radar  
 4 minimum detectable signal of -50 dBZ, the minimum detectable ice water content is on  
 5 the order of  $0.002 \text{ g m}^{-3}$ . The time resolution of the remote sensing data is approximately  
 6 1 min which corresponds to a horizontal wind-advection distance of 800 m.

#### 7 **4. Case specifications**

8 Because of the role of the ocean surface fluxes in cloud formation, it was assumed that  
 9 models were above an ocean surface with forcing specified in the manner of previous  
 10 GCSS boundary layer cloud working group intercomparisons (Stevens et al. 2005, Zhu et  
 11 al. 2005). The initial condition for all models was a cloud-topped boundary layer that was  
 12 well-mixed and capped by an inversion. In terms of the ice-liquid-water potential  
 13 temperature  $\theta_{li}$  and total water mixing ratio  $q_t$ , which are conserved variables under  
 14 adiabatic conditions, these initial conditions were specified as:

$$15 \quad \theta_{li} = \begin{cases} 269.2\text{K} & \text{for } p > p_{inv} \\ 275.33\text{K} + 0.0791 \text{ K hPa}^{-1} \times (815 \text{ hPa} - p) & \text{for } p < p_{inv} \end{cases} \quad (1)$$

$$16 \quad q_t = \begin{cases} 1.95 \text{ g kg}^{-1} & \text{for } p > p_{inv} \\ 0.291 \text{ g kg}^{-1} + 0.00204 \text{ g kg}^{-1} \text{ hPa}^{-1} \times (p - 590 \text{ hPa}) & \text{for } p < p_{inv} \end{cases} \quad (2)$$

1 where  $p$  is atmospheric pressure and  $p_{inv}$  is the inversion pressure with a value of 850  
2 hPa. The total water mixing ratio  $q_t$  is defined as  $q_t = q_v + q_l + q_i$ , where  $q_v$ ,  $q_l$  and  $q_i$   
3 are the mixing ratios of water vapor, liquid water and ice water, respectively. The  
4 definition of  $\theta_{li}$  used here is:

$$5 \quad \theta_{li} = T \times (p_0/p)^{R_d/c_p} \times \exp(-(L_v q_l + L_s q_i)/c_p T_{cb}) \quad (3)$$

6 where  $T$  is the absolute temperature,  $p_0$  is a reference pressure of 1000 hPa,  $T_{cb}$  is the  
7 cloud base temperature of 263K,  $R_d$  is the dry air gas constant,  $c_p$  is the specific heat  
8 capacity of dry air at constant pressure,  $L_v$  and  $L_s$  are the latent heats of vaporization and  
9 sublimation, respectively. Figure 2 displays the initial conditions of the potential  
10 temperature and the mixing ratios of water vapor and liquid water which are consistent  
11 with (1) and (2).

12 Note that the initial phase of the cloud was specified to be pure liquid. It was assumed  
13 that the microphysics present in the model would develop ice during the simulation and  
14 that a microphysical steady state would occur after a few hours of model spin-up. The  
15 lower boundary condition was specified as an ocean surface with temperature 274.01K.  
16 Models were asked to simulate the 12 hr starting from 17Z 9 October 2004.

17 For advective forcing of models in an Eulerian system, one must specify the horizontal  
18 advection of temperature and water vapor as well as the vertical velocity from which  
19 models can calculate the vertical advection of temperature and water vapor. These

1 forcings were based upon analysis data from the European Centre for Medium-Range  
 2 Weather Forecasts (ECMWF) for the ocean region 200 km upstream from the coastline  
 3 between Barrow and Oliktok Point. The ECMWF data for these forcings were idealized  
 4 to:

$$5 \quad -\vec{V} \cdot \nabla T = \min [-4, -15 \times (1 - ((p_s - p)/218.18 \text{ hPa}))] \quad \text{K day}^{-1} \quad (4)$$

$$6 \quad -\vec{V} \cdot \nabla q_v = \min [-0.164, -3 \times (1 - ((p_s - p)/151.71 \text{ hPa}))] \quad \text{g kg}^{-1} \text{ day}^{-1} \quad (5)$$

$$7 \quad \omega = \min [D \times (p_s - p), D \times (p_s - p_{inv})] \quad (6)$$

8 where  $-\vec{V} \cdot \nabla T$  is the temperature tendency from horizontal advection,  $-\vec{V} \cdot \nabla q_v$  is the  
 9 mixing ratio tendency from horizontal advection, and  $\omega$  is the vertical pressure velocity  
 10 (Figure 3). In these equations,  $p_s$  is the surface pressure and  $D$  is the large-scale  
 11 divergence with values of 1010 hPa and  $5.8 \times 10^{-6} \text{ s}^{-1}$ , respectively. The idealization of  
 12 the ECMWF data was made in order to have vertically smooth forcing profiles that  
 13 minimize drifts in the temperature and water vapor above the boundary layer.

14 Lacking in-situ observations and in order to minimize model differences, the surface  
 15 fluxes are specified from ECMWF data with values of  $136.5 \text{ W m}^{-2}$  for sensible heat and  
 16  $107.7 \text{ W m}^{-2}$  for latent heat. While significant uncertainties exist regarding the actual  
 17 magnitudes of these fluxes, sensitivities studies altering these fluxes by  $\pm 25\%$  in the  
 18 UCLA CRM alter the simulated liquid and ice water paths by up to 30% and 50%,  
 19 respectively (Luo et al. 2008a). These differences are smaller than the differences among  
 20 models and between models and observations as shown below. The surface fluxes imply



1 a turbulent boundary layer as the convective velocity scale (Stull 1988, p. 355) is  
2 approximately  $1 \text{ m s}^{-1}$ . Furthermore, radiation calculations with the observed cloud  
3 (Section 6g) suggest that there is a significant longwave radiative cooling of  $70 \text{ W m}^{-2}$  at  
4 cloud top. With turbulence being forced from below and above, it is not surprising that  
5 the boundary layer is approximately well-mixed. One confirmation of the turbulent nature  
6 of the boundary layer is that the SHUPE-TURNER cloud radar retrievals indicate that the  
7 inter-quartile range of vertical velocity inside the cloud is  $0.8 \text{ m s}^{-1}$  (Figure 5c of Shupe  
8 et al. 2008).

9 Besides the buoyancy forcing from the top and bottom of the boundary layer, strong  
10 horizontal winds were present which imply a significant surface stress which also induces  
11 mixing. Models were asked to maintain the mean boundary layer wind close to the  
12 observed values of  $-13 \text{ m s}^{-1}$  in the zonal direction and  $-3 \text{ m s}^{-1}$  in meridional direction  
13 and most models used nudging to accomplish this.

14 Radiation calculations in both the solar and longwave portion of the spectrum were  
15 performed by each model using their own predicted atmospheric state and radiation  
16 parameterization. The calculated radiative heating rates affect the evolution of the  
17 atmosphere and in particular, cloud-top radiative cooling can drive atmospheric  
18 circulations. Surface radiative fluxes do not affect surface temperatures, because the  
19 surface temperature and heat fluxes are specified. However, these radiative fluxes are  
20 compared with observations to assess the fidelity of model simulations.

1 The following aerosol characteristics, more fully discussed in Morrison et al. (2008a),  
2 were recommended to the models that have an explicit aerosol-cloud coupling. For the  
3 aerosol size distribution, a bimodal lognormal dry aerosol size distribution was fitted to  
4 the available observations. The size distribution for each mode is given by

$$5 \quad \frac{dN}{d \ln r} = \frac{N_t}{\sqrt{2\pi} \ln \sigma} \exp\left[-\frac{\ln^2(r/r_m)}{2 \ln^2 \sigma}\right] \quad (7)$$

6 where  $N$  is the number concentration of aerosols and  $r$  is the particle radius. The  
7 parameters  $N_t$ ,  $r_m$ , and  $\sigma$  are total number concentration, geometric mean radius, and  
8 standard deviation of each particle mode. For the smaller particle mode, these parameters  
9 have values of  $72.2 \text{ cm}^{-3}$ ,  $0.052 \text{ }\mu\text{m}$ , and  $2.04$ , respectively. For the larger particle mode,  
10 these parameters have values of  $1.8 \text{ cm}^{-3}$ ,  $1.3 \text{ }\mu\text{m}$ , and  $2.5$ , respectively. The aerosol  
11 composition was assumed to be ammonium bisulfate with an insoluble fraction of about  
12 30% (Fridlind et al. 2000).

13 The amount of ice nuclei is an important parameter for models that simulate the number  
14 concentration of ice crystals. The Continuous Flow Diffusion Chamber on the Citation  
15 measured the ice nuclei with a diameter less than  $2 \text{ }\mu\text{m}$  acting in deposition,  
16 condensation-freezing, and immersion-freezing modes (Prezzi et al. 2007). No  
17 measurement of ice nuclei acting in contact mode was possible. The measurements  
18 indicate extremely low amounts of ice nuclei with 85% of measurements having ice  
19 nuclei beneath background levels of  $0.1 \text{ L}^{-1}$  (Verlinde et al. 2007). Of the measurements

1 with ice nuclei above background, the maximum concentration was about  $10 \text{ L}^{-1}$ . The  
2 mean of all observations including those beneath background levels was  $0.16 \text{ L}^{-1}$ .

3 More information on the intercomparison specifications and plots of model simulations  
4 and observational data are available from  
5 <http://science.arm.gov/wg/cpm/scm/scmic5/index.html>.

## 6 **5. Model descriptions**

### 7 a. Overview

8 Tables 1 & 2 encapsulate the relevant characteristics of the seventeen SCMs and nine  
9 CRMs that took part in this intercomparison.

10 Among the SCMs, there are versions of two operational weather prediction models  
11 (ECMWF and NCEP) and five operational climate models (CCCMA, ECHAM, GFDL,  
12 GISS, and SCAM3). There are four SCMs which have primarily been used in research  
13 studies (ARCSCM, MCRAS, SCRIPPS, and UWM). Finally, there are six SCMs which  
14 include single modifications of the base set of SCMs (ECMWF-DUALM, GISS-LBL,  
15 MCRASI, SCAM3-LIU, SCAM3-MG, and SCAM3-UW). Four of these six include  
16 modifications to the representation of cloud microphysics: three SCMs add double  
17 moment microphysics (MCRASI, SCAM3-LIU, and SCAM3-MG) and one adds bin  
18 resolved cloud microphysics (GISS-LBL). Two of these six include modifications to the  
19 representation of boundary layer turbulence (ECMWF-DUALM and SCAM3-UW). The

1 number of vertical levels in the boundary layer varies from four to fifty-one with a  
2 median value of seven.

3 Among the CRMs, five are two-dimensional (NMS-BULK, NMS-SHIPS, RAMS-CSU,  
4 UCLA-LARC, UCLA-LARC-LIN), and four are three-dimensional (COAMPS<sup>®</sup>,  
5 DHARMA, METO, and SAM). There is a wide variety of horizontal and vertical  
6 resolutions as well as total domain represented. The two-dimensional models typically  
7 have horizontal and vertical resolutions of order 1000 m and 100 m, respectively,  
8 whereas the three-dimensional models typically have horizontal and vertical resolutions  
9 of 50 m in both directions. The number of vertical levels in the boundary layer varies  
10 from seven to seventeen for the two-dimensional models and from twenty-seven to sixty-  
11 four for the three-dimensional models. Total domain size is order 100 km for the two-  
12 dimensional models and 5000 m by 5000 m for the three-dimensional models. Thus,  
13 configurations of the two-dimensional models are typical of models commonly referred  
14 to as “cloud-resolving models” whereas the configurations of the three-dimensional  
15 models are typical of models commonly referred to as “large-eddy simulations”.

#### 16 b. Cloud microphysics

17 As the representation of cloud microphysics may be central to the ability of models to  
18 simulate a mixed-phase cloud, a brief summary of the microphysics used in these models  
19 is now given. Readers seeking more detail should consult the references in Tables 1 and  
20 2.

1 The parameterizations of cloud microphysics can be classified into four categories  
2 which span the range of detail used in today's cloud models. The simplest representation,  
3 which will be called "single moment with T-dependent partitioning", employs a single  
4 prognostic variable for the mass of cloud condensate and uses a temperature-dependent  
5 function to partition the relative amounts of liquid and ice. The relative amount of liquid  
6 at the cloud-top temperature of  $-15^{\circ}\text{C}$  varies from 12% to 83% in the six SCMs  
7 (ECMWF, ECMWF-DUALM, MCRAS, NCEP, SCAM3, SCAM3-UW) and one CRM  
8 (SAM) that have this type of microphysical representation. Note that SAM also employs  
9 a temperature-dependent partitioning to determine the relative amounts of rain, snow, and  
10 graupel which at  $-15^{\circ}\text{C}$  are 0%, 42%, and 58%, respectively.

11 The second class of cloud microphysics, "single moment with independent liquid and  
12 ice", employs separate prognostic variables for the mass of cloud liquid and ice in which  
13 the relative amounts of liquid and ice are not solely a function of temperature. Five SCMs  
14 (CCCMA, GFDL, GISS, SCRIPPS, and UWM) and one CRM (UCLA-LARC-LIN)  
15 employ this class of microphysics. In these models, the considerations which determine  
16 the relative amounts of liquid and ice typically include a temperature dependent  
17 partitioning of liquid and ice at cloud formation and subsequent conversion of liquid to  
18 ice through riming, droplet freezing, or the Bergeron-Findeisen process which in mixed-  
19 phase clouds favors the growth of ice over liquid due to ice's lower saturation vapor  
20 pressure.

1 The third class of cloud microphysics, “double moment”, employs prognostic variables  
2 for both the mass of condensate as well as the number concentration of cloud particles.  
3 Five SCMs (ARCSCM, ECHAM, MCRASI, SCAM3-LIU, SCAM3-MG) and five  
4 CRMs (COAMPS<sup>®</sup>, METO, NMS-BULK, RAMS-CSU, UCLA-LARC) employ this  
5 approach. An advantage over the previous two classes is that a prognostic representation  
6 of number concentration potentially allows for a physically based coupling of clouds with  
7 aerosols. While not every condensate species may be represented with a prognostic  
8 variable for number concentration, all double moment parameterizations in this study  
9 represent the number concentration of cloud (or small) ice with a prognostic variable.

10 The fourth class of cloud microphysics, “bin microphysics”, represents the number  
11 concentration of particles of different sizes with prognostic variables. This is the most  
12 complete representation of microphysics used in this study and is used in one SCM  
13 (GISS-LBL) and two CRMs (DHARMA and NMS-SHIPS). In DHARMA and NMS-  
14 SHIPS, twenty size bins each are used to represent liquid and ice particles. DHARMA  
15 has forty additional size bins for the mass of dissolved solute in each of the liquid drop or  
16 ice crystal size bins. GISS-LBL uses thirty-three size bins to represent liquid droplets and  
17 six classes of solid or partially solid condensate which include plates, columns, dendrites,  
18 snow, graupel, and frozen drops.

19 Further discussion of the widely-varying treatment of ice microphysics in models is  
20 warranted because previous studies have demonstrated the critical importance of ice  
21 microphysics in simulations of Arctic mixed-phase clouds, especially representation of

1 the vapor depositional growth of ice and the Bergeron-Findeisen process (e.g.,  
2 Harrington 1999; Morrison and Pinto 2006; Prenni et al. 2007). Single-moment schemes  
3 with T-dependent partitioning do not explicitly treat ice initiation and conversion of cloud  
4 liquid water to ice and instead fix the ratio of liquid and ice as a function of temperature.  
5 Most of the single-moment schemes with independent liquid and ice and all of the two-  
6 moment and bin schemes explicitly represent the Bergeron-Findeisen process and most  
7 include additional liquid-ice conversion processes via heterogeneous droplet freezing. In  
8 the more detailed one-moment schemes (GFDL, UCLA-LARC-LIN, UWM) and all of  
9 the two-moment and bin schemes, the Bergeron-Findeisen process depends on the  
10 specified or predicted crystal concentration as well as other ice microphysical parameters  
11 (e.g., capacitance). It is this dependence that has led to significant sensitivity of mixed-  
12 phase cloud simulations to treatment of the crystal concentration in previous studies (e.g.,  
13 Pinto 1998; Harrington et al. 1999; Jiang et al. 2000; Morrison et al. 2003; Morrison and  
14 Pinto 2006; Prenni et al. 2007).

15 The crystal concentration is specified in single-moment schemes and this specification  
16 varies widely among the participating models. In the two-moment and bin schemes the  
17 crystal concentration is predicted and evolves through various source (primary ice  
18 nucleation and secondary ice multiplication) and sink (aggregation, sedimentation) terms.  
19 In all of the simulations shown here, primary ice nucleation is the dominant source and  
20 secondary ice multiplication is of limited importance. Ice nucleation occurs via several  
21 mechanisms (contact and immersion freezing, deposition, and condensation-freezing),  
22 although their representation differs widely among the models. As shown in section 6e,

1 the different treatments of ice nucleation are associated with large differences in the  
2 simulated ice crystal concentrations. Most of the models treat the ice nuclei concentration  
3 diagnostically, although two of the models (DHARMA and RAMS-CSU) prognose this  
4 quantity. Several of the models with diagnostic ice nuclei scaled their values to those  
5 observed in M-PACE (ARCSCM, ECHAM, GISS-LBL, NMS-BULK, SCAM-MG,  
6 UCLA-LARC). However, other models used their default ice nuclei concentrations, such  
7 as the formulation from Meyers et al. (1992) which predicts far greater amounts of ice  
8 nuclei than observed. Even among the models that scaled their ice nuclei concentrations  
9 to the observations, this scaling was not applied to all of the nucleation mechanisms  
10 parameterized in the models.

11 In general, only models with double moment or bin microphysics represent the  
12 dependence of cloud properties on aerosols. However, three models with double moment  
13 parameterizations of cloud microphysics do not have an explicit dependence of cloud  
14 properties on aerosols (COAMPS<sup>®</sup>, METO, NMS-BULK). Of the twelve models in  
15 which cloud properties depend on aerosols (ARCSCM, CCCMA, DHARMA, ECHAM,  
16 GISS-LBL, MCRAS, MCRASI, NMS-SHIPS, RAMS-CSU, SCAM3-LIU, SCAM3-MG,  
17 UCLA-LARC), two models couple only the liquid-phase microphysics (CCCMA and  
18 MCRAS) while two others couple only the ice-phase microphysics (NMS-SHIPS and  
19 RAMS-CSU). In all models except DHARMA and RAMS-CSU which prognose ice  
20 nuclei, aerosols are fixed in time and thus a two-way coupling of aerosols and clouds is  
21 not present.



## 1 **6. Results**

### 2 a. Cloud and hydrometeor fraction

3 Figure 4 displays the height profile of the average cloud fraction from the observations  
4 and model simulations. For the observations, one of the profiles is deduced from the  
5 ground-based remote sensors at Barrow (SHUPE-TURNER) and the other two are from the  
6 two aircraft flights during the period. The aircraft cloud fraction depicts the fraction of  
7 time in a flight in which a given altitude was between cloud base and cloud top. For the  
8 remote sensors, cloud top is defined as the altitude of the highest range gate with  
9 significant radar return and cloud base is defined from the laser ceilometer which  
10 corresponds in this case to the lowest altitude with a significant amount of liquid water.  
11 For the aircraft, cloud top is defined as the highest altitude with cloud liquid or ice and  
12 cloud base is defined as the lowest altitude with liquid water where the presence of liquid  
13 or ice is determined by the approximate threshold value for detectable water content of  
14  $0.001 \text{ g m}^{-3}$  (McFarquhar et al. 2007b).

15 Figure 4 indicates that the cloud bases and tops and cloud thicknesses are greater in the  
16 retrievals from the ground-based remote sensors at Barrow than they are in those  
17 determined from the aircraft data. Some of these differences are due to a strong east-west  
18 gradient in cloud top, base and thickness which was observed by the aircraft which flew  
19 between Oliktok Point and Barrow. For example, the easternmost spirals near Oliktok  
20 Point in both flights have cloud tops of 950 to 1000 m whereas the westernmost spirals  
21 near Barrow have cloud tops of 1300 to 1500 m. The east-west gradient in geometrical

1 cloud thickness is consistent with the greater liquid water path retrieved from the  
2 microwave radiometer at Barrow relative to that of Oliktok Point (Table 3). It is also  
3 consistent with the satellite image of Figure 1 which shows that the typical roll width,  
4 which is generally positively correlated to the depth of the boundary layer, is greater at  
5 Barrow than at Oliktok Point.

6 Similar to the observations, SCMs and CRMs produce a solid cloud layer between 700  
7 and 1300 m (Figure 4). To construct each model cloud fraction panel, the cloud fraction  
8 for each model was averaged over the 12 hr simulation omitting the first 3 hr for model  
9 spin-up. From the set of cloud fraction profiles, the values of cloud fraction at each height  
10 which correspond to the median, minimum, maximum and 25<sup>th</sup> and 75<sup>th</sup> percentiles of  
11 models were calculated at each altitude. The model panels show the median cloud  
12 fraction (solid black line), the inner 50% of models (the darker shaded area), and the  
13 range of the data (the area of both the lighter and darker shading). All CRMs were asked  
14 to compute cloud fraction which was defined as the fraction of grid volumes with cloud  
15 droplet mixing ratios greater than 0.01 g kg<sup>-1</sup> or ice mixing ratios greater than 0.0001 g  
16 kg<sup>-1</sup>. Unfortunately, these thresholds differ from those of the aircraft or ground-based  
17 remote sensors (Section 3) which were determined at a later time than when this  
18 intercomparison began; however, the differences in thresholds are not likely to have a  
19 great impact on the statistics of the cloud and hydrometeor fraction, and have little or no  
20 impact on the other diagnostics examined in this paper. For SCMs, cloud fraction is an  
21 inherent property of the model which is generally thought to mean the horizontal fraction  
22 of a grid-cell that is saturated and contains either cloud liquid or ice.

1 Both the observed and modeled clouds produced precipitation. This is shown in a plot of  
2 the hydrometeor fraction (Figure 5), which is defined as the area fraction which contains  
3 either cloud or precipitation. From the observations, this was calculated using the  
4 presence of any liquid or ice condensate from the remote sensor retrievals. For the  
5 models, this was calculated using either the presence of cloud, as defined above, or rain,  
6 snow, or graupel mixing ratios in excess of  $0.0001 \text{ g kg}^{-1}$ . The remote sensors indicate  
7 that the cloud continually produced precipitation which reached the surface.

8 As to the phase of the hydrometeors, the phase classifications from the aircraft data and  
9 the remote sensors (SHUPE-TURNER) are consistent (Figure 6). This figure displays the  
10 fraction of time that a given phase occurred composited on a normalized height  
11 coordinate where  $-1$  is the surface,  $0$  is cloud base, and  $+1$  is cloud top. The observations  
12 indicate most of the cloud is mixed-phase (liquid and ice co-existing in the same volume)  
13 with ice-phase precipitation beneath the cloud. Liquid-phase only condensate is detected  
14 on occasion near the cloud top.

#### 15 b. Liquid and ice water path

16 Although models generally produce an overcast precipitating cloud, substantial  
17 differences exist in the simulated phase partitioning and mass of cloud condensate. Figure  
18 7 shows a scatterplot of the median liquid water and ice water paths from the  
19 observations and the models. The observations are indicated by the letters on the plot: 'A'  
20 for aircraft data, 'S' for SHUPE-TURNER retrievals, and 'W' for WANG retrievals. The  
21 models are displayed with symbols that categorize a given model according to whether it

1 is a SCM or CRM which is indicated by the symbol filling and the class of its  
2 microphysical scheme which is indicated by the symbol shape. Medians and inter-quartile  
3 ranges of the observational data are presented in Table 3 and results from individual or  
4 subsets of models are presented in Table 4.

5 Because the observations do not distinguish cloud from precipitation condensate, the  
6 vertical integrals of the model condensate include precipitation condensate in the reported  
7 liquid and ice water paths. For the liquid-phase, the contribution of rain to the total water  
8 path is always much smaller than the contribution of cloud droplets, whereas for the ice-  
9 phase, the contribution of snow is often equal to or larger than the contribution of the  
10 small ice. Graupel makes little or no contribution to the total ice water path in the CRMs.  
11 Note that for the SCMs, the contribution of rain and snow must be calculated from the  
12 vertical profiles of the precipitation rate as the mixing ratios of rain and snow are  
13 generally not prognostic variables in SCMs. These precipitation rates were unavailable  
14 from some SCMs (ECHAM, GISS, McRAS, McRASI, NCEP, and SCRIPPS).

15 The observations indicate that the cloud system was water dominated. The retrievals from  
16 the ground-based remote sensors at Barrow indicate a liquid water path of about  $200 \text{ g m}^{-2}$   
17 <sup>2</sup>, whereas the aircraft liquid water path, which is determined from a vertical integral of  
18 the profile data, is lower with values around  $120 \text{ g m}^{-2}$ . As mentioned previously, some  
19 of this difference reflects the east-west gradient in cloud properties; this is further  
20 confirmed by the liquid water paths retrieved from the microwave radiometers at Oliktok  
21 Point which have values around  $100 \text{ g m}^{-2}$  (Table 3) which is about one-half of the value

1 at Barrow. For the ice-phase, both the SHUPE-TURNER and WANG retrievals at Barrow  
2 suggest  $30 \text{ g m}^{-2}$  of ice whereas the aircraft observations suggest far lower values of  
3 around  $5 \text{ g m}^{-2}$ . In addition to the east-west gradient in cloud properties, some of this  
4 difference arises because the aircraft totals do not include ice from the lower 60% of sub-  
5 cloud air which the aircraft did not sample (Figure 6). Taking into account these factors  
6 as well as the uncertainty in the measurements (Section 3), a best estimate of the liquid  
7 and ice water paths for this period and region would be  $160 \pm 50 \text{ g m}^{-2}$  and  $15 \text{ g m}^{-2} \pm$  a  
8 factor of two (i.e., the ice water path could be between 8 and  $30 \text{ g m}^{-2}$ ), respectively.

9 The model simulations produce a wide range of results. Although more than three-  
10 quarters of the models have liquid water paths in excess of ice water paths as observed,  
11 two-thirds of the models underestimate the observed liquid water path. The median liquid  
12 and ice water paths differ little according to model type with values of  $56.0 \text{ g m}^{-2}$  and  
13  $57.3 \text{ g m}^{-2}$  for the liquid-phase from SCMs and CRMs, respectively, and values of  $29.1 \text{ g}$   
14  $\text{m}^{-2}$  and  $17.1 \text{ g m}^{-2}$  for the ice-phase from SCMs and CRMs (Table 4). Thus, on average,  
15 the primary model deficiency is an underestimate of the amount of liquid present in the  
16 clouds. Despite this general underestimate, five models (DHARMA, SCAM3, SCAM3-  
17 LIU, SCAM3-UW, and UCLA-LARC) have liquid and ice water paths which are  
18 consistent with the best estimate of the observations, which is indicated by the lightly  
19 dashed rectangle in Figure 7. Two of these models (SCAM3 and SCAM3-UW) achieve  
20 good results in part because their specified temperature-dependent partitioning of liquid  
21 and ice yields a cloud with 83% liquid at  $-15^\circ\text{C}$  in rough agreement with the  
22 observations. However, the SCAM3 performs poorly for the simulation presented in Part

1 II where a different ratio of liquid to ice was observed in a cloud with a similar  
2 temperature (SCAM3-UW did not participate in Part II). The three other models  
3 (DHARMA, SCAM3-LIU, and UCLA-LARC) which are consistent with the  
4 observations both here and in Part II have more sophisticated cloud microphysics  
5 suggesting that it might be beneficial to more closely examine the role of microphysics in  
6 producing a good simulation.

7 Indeed, the median liquid and ice water paths appear to approach the observed values as  
8 the sophistication of the cloud microphysical parameterization increases. Specifically, the  
9 median liquid water path for the seven models with single moment with T-dependent  
10 partitioning is  $21.2 \text{ g m}^{-2}$ , whereas that for the six models with single moment with  
11 independent liquid and ice microphysics is  $72.8 \text{ g m}^{-2}$ , and that of the ten models with  
12 double moment microphysics is  $100 \text{ g m}^{-2}$ . The corresponding quantities for ice water  
13 path are 33.8, 31.8, and  $19.9 \text{ g m}^{-2}$ , among these models. However, the models with bin  
14 microphysics do not show improvement over the models with double moment  
15 microphysics, but there are only three models with this microphysical class.

16 Despite this general trend, use of a particular class of cloud microphysics does not  
17 guarantee a good simulation. For example, half of the ten models with double moment  
18 microphysics have liquid water paths less than  $60 \text{ g m}^{-2}$ , whereas the other half of these  
19 models have liquid water paths in excess of  $140 \text{ g m}^{-2}$ . The median liquid water path of  
20  $100 \text{ g m}^{-2}$  is thus a statistical average of a bimodal population of models. Undoubtedly,  
21 differences in the representation of boundary layer turbulence or whether it is a SCM or

1 CRM are also responsible for the spread of model results. This is illustrated by  
2 examination of two of the three pairs of models which use identical microphysics but  
3 differ in the formulation of boundary layer turbulence or whether it is a SCM or CRM.  
4 For both of these pairs (ECMWF and ECMWF-DUALM, and ARCSCM and UCLA-  
5 LARC, respectively), the total condensate water path differs by more than  $100 \text{ g m}^{-2}$   
6 demonstrating that the simulated cloud properties depend on more than the cloud  
7 microphysical scheme employed.

8 Aerosol-cloud coupling appears to improve the CRM simulations of liquid water path as  
9 all CRMs with coupling have liquid water paths greater than CRMs without aerosol-  
10 cloud coupling. However, two (NMS-SHIPS and RAMS-CSU) of the four CRMs with  
11 aerosol-cloud coupling produce virtually no ice which in the case of RAMS-CSU is due  
12 to precipitation scavenging of all of the initial ice nuclei. Furthermore, SCMs do not  
13 display stratification of liquid water paths by aerosol-cloud coupling. From this set of  
14 simulations, there does not appear to be a single feature of a model that guarantees a good  
15 simulation of the column integrated amount of liquid and ice; rather, it is likely that a  
16 good cloud simulation depends on several high-quality model components functioning  
17 well together.

### 18 c. Liquid and ice water content

19 The vertical distributions of liquid and ice water content from the observations and  
20 models on a normalized height coordinate are displayed in Figures 8 and 9. The aircraft  
21 measured liquid water content indicates that the liquid water content increases with

1 height above cloud base which is a characteristic of adiabatic clouds in well-mixed  
2 boundary layers. However, the maximum aircraft liquid water content is smaller than the  
3 adiabatic value of the cloud top liquid water content which is  $0.6 \text{ g m}^{-3}$  for a cloud with  
4 the aircraft observed thickness of 600 m. The sub-adiabatic nature of the cloud is  
5 consistent with depletion of liquid water by ice precipitation, although cloud-top  
6 entrainment may also contribute to the depletion. Because the vertical profile of liquid  
7 water content in mixed-phase clouds cannot currently be retrieved, no remote sensing  
8 panel for liquid water content is displayed in Figure 8. Despite this, the remote sensor  
9 retrievals also indicate that the cloud at Barrow is less than adiabatic as the retrieved  
10 liquid water path of  $195$  to  $225 \text{ g m}^{-2}$  is smaller than the adiabatic liquid water path which  
11 is between  $235$  and  $270 \text{ g m}^{-2}$  for the observed cloud thicknesses of  $700$  to  $750$  m at  
12 Barrow. Both SCMs and CRMs simulate greater liquid water content in the upper half of  
13 the cloud although this tendency is more apparent for the highest 25% of models than it is  
14 for the model median value. The low vertical resolution of some SCMs hinders a robust  
15 assessment of this point, however. Consistent with the liquid water path, the median  
16 model liquid water content is significantly smaller than observed.

17 The vertical profile of ice water content is generally more uniform than that of the liquid  
18 water content in both the aircraft and retrievals. The aircraft data indicate median values  
19 of  $0.01 \text{ g m}^{-3}$  which are fairly constant in the cloud and the portion beneath the cloud that  
20 the aircraft sampled. The WANG retrievals at Barrow indicate somewhat larger median  
21 values in the cloud than in the layer beneath,  $0.02$  to  $0.03 \text{ g m}^{-3}$  as compared to  $0.01$  to  
22  $0.02 \text{ g m}^{-3}$ . SHUPE-TURNER retrievals are similar. Some of these differences between the



1 aircraft and ground-based retrievals are probably due to the east-west gradient in cloud  
2 properties, although the differences are within the measurement uncertainty (Section 3).  
3 A feature of both the aircraft and ground-based retrievals is that the distribution of ice  
4 water content has a long positive tail with some values in excess of  $0.1 \text{ g m}^{-3}$ . The model  
5 median values are in reasonable agreement with the observations for both the SCMs and  
6 CRMs. The models ice water content values are also somewhat greater in the cloud than  
7 in the layer beneath. A decrease in ice water content as one approaches the surface would  
8 be consistent with sublimation of ice in the sub-saturated layers near the surface. Note  
9 that the ground-based retrievals of ice water content do not decrease in the layer between  
10 normalized height of  $-0.2$  and  $0.0$  (cloud base), consistent with ice super-saturation in the  
11 observed sounding for this layer.

#### 12 d. Surface precipitation

13 The ice reaching the surface will be observed as surface precipitation. Unfortunately  
14 quantitative estimates of the surface snow rate are highly uncertain. The National  
15 Weather Service station in Barrow recorded  $0.25 \text{ mm d}^{-1}$  for this period. However, for an  
16 ice water mixing ratio of  $0.01 \text{ g m}^{-3}$  at the surface (Figure 9) with an assumed mass-  
17 weighted fall speed of  $1 \text{ m s}^{-1}$ , the precipitation rate would be  $0.9 \text{ mm d}^{-1}$ . The median  
18 surface snow rates of SCMs and CRMs are  $0.70$  and  $0.41 \text{ mm d}^{-1}$ , respectively. Although  
19 in most models the surface rain rate is zero or very much smaller than the snow rate, there  
20 are a few models (CCCMA, ECHAM, RAMS-CSU) in which all of the surface

1 precipitation is in the form of rain. These models have a high liquid water path but are  
2 unable to produce enough ice so that ice precipitation would reach the surface.

3 e. Cloud microphysics

4 From the aircraft observations, the median mass-weighted effective radii of liquid and ice  
5 are 10 and 25  $\mu\text{m}$ , respectively, and the median mass-weighted number concentrations of  
6 liquid and ice are 38  $\text{cm}^{-3}$  and 2  $\text{L}^{-1}$ , respectively. While the ice crystal number  
7 concentration of 2  $\text{L}^{-1}$  is an order of magnitude larger than the measured ice nuclei  
8 concentration (Section 4), it is in agreement with previous aircraft observations in Arctic  
9 clouds with similar temperatures (Jayaweera and Ohtake 1973, Pinto 1998, Gultepe et al.  
10 2001). As an aside, the reader should consult Fridlind et al. (2007) for possible reasons  
11 the ice crystal concentration is greater than the ice nuclei concentration. These aircraft  
12 observations were compared to model simulations. Unfortunately, general conclusions  
13 about the ability of models to reproduce the observations cannot be made due to the very  
14 wide range of model results from the roughly 50% of models which submitted the  
15 relevant diagnostics.

16 As an example, the relationship between ice number concentration and liquid water path  
17 is examined to ask the question do the model-simulated liquid water paths exhibit the  
18 inverse relationship with ice number concentration found in prior studies (e.g.,  
19 Harrington et al. 1999; Jiang et al. 2000; Morrison and Pinto 2006; Prenni et al. 2007)?  
20 Although ice crystal number concentrations vary over five orders of magnitude among  
21 models, the expected inverse relationship is not clearly shown from a scatterplot of ice

1 number concentration and liquid water path (Figure 10). Contrary to expectations, four  
2 models with ice number less than  $10 \text{ L}^{-1}$  have liquid water paths less than  $30 \text{ g m}^{-2}$  and  
3 one model with a high ice number concentration of  $350 \text{ L}^{-1}$  has a liquid water path of  $165$   
4  $\text{g m}^{-2}$  consistent with the observations. However, in this one model (ECHAM), the high  
5 ice number concentration has no direct impact on the liquid water path because the ice  
6 specific humidity never exceeds a model-imposed threshold of  $0.0005 \text{ g kg}^{-1}$  required to  
7 activate the Bergeron-Findeisen process. Clearly, ice number concentration is only one  
8 factor of many influencing the ability of a model to simulate a mixed-phase cloud. Some  
9 caution with regard to this figure should be taken as it is not clear that all modelers  
10 limited the count of their ice crystal number to particles with diameters greater than  $53$   
11  $\mu\text{m}$  as was done with the observations (McFarquhar et al. 2007b). Nonetheless, the  
12 treatment of model diagnostics is unlikely to explain the very large range of simulated ice  
13 number concentrations which most likely results from the widely-varying treatment of ice  
14 nucleation among the models.

15 Indeed, the differences in ice number concentration between the two models that  
16 prognose ice nuclei (RAMS-CSU and DHARMA) can likely be explained by differences  
17 in the modeling of processes that affect ice nuclei. In RAMS-CSU, nearly all of the initial  
18 ice nuclei are consumed by ice precipitation in a few hours resulting in the lowest ice  
19 number concentration of the set ( $0.003 \text{ L}^{-1}$ ). A similar result was initially found in  
20 DHARMA using standard microphysical treatments, however the non-standard inclusion  
21 of a process whereby ice nuclei are formed in a very tiny fraction of cloud droplet  
22 evaporation events leads to larger and sustainable ice number concentrations ( $4 \text{ L}^{-1}$ ) as

1 well as decrease in liquid water path from around 220 to 135 g m<sup>-2</sup> (Fridlind et al. 2007,  
2 note that the model described as “Evaporation nuclei” in their Table 2 was submitted for  
3 this intercomparison).

#### 4 f. Thermodynamic structure

5 Figure 11 compares the time-averaged profiles of total water mixing ratio  $q_t$  and ice-  
6 liquid water potential temperature  $\theta_{li}$  from the model simulations to the initial condition.  
7 The model underestimate of liquid water content is consistent with a reduction of  $q_t$  in the  
8 upper half of the boundary layer and a vertical gradient of  $q_t$  which differs from the initial  
9 conditions and is likely unrealistic. Note that a cloud with a liquid water content of two-  
10 thirds of the adiabatic value but a water vapor mixing ratio which follows the adiabatic  
11 profile of the initial condition (Figure 2) would have a value of  $q_t$  at cloud top that is  
12 only 0.15 g kg<sup>-1</sup> lower than the value in the sub-cloud layer.

13 Ice precipitation would in absence of other effects try to stabilize the boundary layer by  
14 providing a net heating to the cloud layer and a net cooling to the sub-cloud layer.  
15 Although there is some evidence for stabilization in the CRM profiles of  $\theta_{li}$ , the surface  
16 fluxes and cloud-top radiative cooling in models with a significant amount of liquid act to  
17 keep the boundary layer well-mixed and probably minimize the influence of ice  
18 precipitation on vertical stability. Models which have greater amounts of cloud liquid  
19 water content do show smaller vertical gradients in  $q_t$  and  $\theta_{li}$ .

1 g. Radiation

2 Figure 12 compares models simulations of the solar transmission to the radiation  
3 measurements at Barrow (OBS) and the results of two calculations from a radiative  
4 transfer model (STREAMER, Key and Schweiger 1998) that uses the initial condition  
5 sounding of temperature and water vapor and along with cloud liquid and ice water paths  
6 of 200 and 13 g m<sup>-2</sup>, respectively. The solar transmission is computed as the average  
7 value for the period 17Z 9 October to 5Z 10 October 2004 of the downward shortwave  
8 radiative flux at the surface divided by that at the top-of-atmosphere. The solar  
9 transmission is plotted together with the total condensate water path, although it is  
10 understood that there are a number of reasons for why the points will not scatter along a  
11 single line. As might be expected from the model underestimate of liquid water path,  
12 models generally overestimate the solar transmission.

13 The model overestimate is greater than it appears because model simulations used an  
14 ocean surface. Given that the observations were over snow-covered land at Barrow, the  
15 observed solar transmission is enhanced by multiple reflections between the surface and  
16 the cloud. The impact of the different surface albedo can be assessed by comparing  
17 STREAMER calculations that use an ocean surface with low albedo (S-O) to those that  
18 use a snow-covered land surface with high albedo (S-L). Given that STREAMER  
19 calculations with the land surface have good agreement with the observations, it suggests  
20 that models should simulate solar transmissions closer to 0.1 than to 0.2.

1 In the Arctic, the downward component of longwave radiation at the surface is strongly  
2 affected by clouds and is an important quantity that affects the surface temperature of  
3 over land and sea-ice. Although the surface temperature is fixed in these model  
4 simulations, it is still important to assess whether the simulated cloud has the correct  
5 effect on surface fluxes of radiation. STREAMER calculations with the observed cloud,  
6 either over an ocean or land surface, are consistent with the observed value of  $280 \text{ W m}^{-2}$   
7 (Figure 13). As the downward longwave radiation is  $200 \text{ W m}^{-2}$  in clear-sky  
8 STREAMER calculations, the longwave cloud radiative effect is about  $80 \text{ W m}^{-2}$ . Given  
9 that the longwave emissivity of clouds is near unity after the condensate water path  
10 exceeds about  $50 \text{ g m}^{-2}$  (Stephens 1978), it would be expected and is found that models  
11 with total condensate water paths greater than this value produce longwave cloud  
12 radiative effects consistent with the observations (Figure 13).

## 13 **7. Sensitivity studies**

### 14 a. No ice microphysics

15 Given that numerous modeling studies (Pinto 1998; Harrington et al. 1999; Jiang et al.  
16 2000; Morrison and Pinto 2006; Prenni et al. 2007) have demonstrated that the amount of  
17 supercooled water in mixed-phase clouds is very sensitive to the representation of ice  
18 microphysics in general, and to the ice crystal number concentration in particular, it is of  
19 interest to determine this sensitivity with the present set of models. A sensitivity study  
20 was performed in which models were asked to simulate a hypothetical case of a liquid-  
21 phase cloud. A sensitivity study focused on the ice crystal number concentration was not

1 performed because the liquid-only phase experiment is simple to construct and permits  
2 all models to perform a meaningful simulation.

3 The results demonstrate that there is a large sensitivity of the integrated amount of  
4 condensate to the inclusion of ice microphysics (Figure 14). However, this is only true in  
5 the models which have condensate water paths less than  $150 \text{ g m}^{-2}$  in the control  
6 simulation. In these models, the condensate water path in the no ice microphysics  
7 experiment is greater than that of the control simulation and is often between 200 and 300  
8  $\text{g m}^{-2}$ . At least in these models, this suggests that excessive conversion of liquid to ice  
9 which easily precipitates is responsible for the underestimate of liquid water path. This is  
10 partially confirmed by Figure 15 which shows a general tendency for models which have  
11 a high fraction of ice in the control experiment to show the greatest relative increase in  
12 the condensate water path.

13 The spread in liquid water path among the SCMs and CRMs is still large in the no ice  
14 microphysics experiment. SCM liquid water paths vary from 60 to  $580 \text{ g m}^{-2}$ , while  
15 CRM liquid water paths vary from 65 to  $330 \text{ g m}^{-2}$ . This indicates that differences in the  
16 representation of processes such as liquid-phase microphysics and boundary layer  
17 turbulence can still lead to significant differences in the simulated liquid water path.

18 For the models which are sensitive to the inclusion of ice-phase microphysics, the  
19 boundary layer tends to be more well-mixed in  $q_t$  and  $\theta_i$  relative to the same model in  
20 the control experiment and in the sensitive CRMs the boundary layer is slightly deeper.

1 These effects are likely due to greater turbulence near cloud top which is driven by  
2 strong cloud top radiative cooling common to stratocumulus.

### 3 b. Vertical resolution

4 Low vertical resolution in atmospheric models in general, and climate models in  
5 particular, may lead to non-convergence of simulated cloud properties. Yuan et al. (2006)  
6 found a significant decrease in the liquid and ice water paths as vertical resolution was  
7 increased in CCCMA SCM simulations of mixed-phase clouds observed during SHEBA.  
8 Models were asked to submit a simulation with higher vertical resolution. As the vertical  
9 resolution in this sensitivity study was not specified, the number of levels in the boundary  
10 layer varied from 14 to 146 in the SCMs and from 23 to 53 in the CRMs (Tables 1 and  
11 2). Reassuringly, the results indicate a fairly small sensitivity to vertical resolution which  
12 is generally much less than the sensitivity to the inclusion of ice microphysics (compare  
13 Figure 16 to Figure 14). One SCM (SCAM3-LIU) did exhibit a pronounced sensitivity of  
14 cloud phase to vertical resolution (Table 4). This was due to a bug in the ice nucleation  
15 parameterization which has subsequently been corrected.

## 16 **8. Summary**

17 An intercomparison of single-column and cloud-resolving model simulations of cold-air  
18 outbreak mixed-phase stratocumulus has been presented and evaluated with the available  
19 ground-based and aircraft observations collected during the ARM Mixed-Phase Arctic  
20 Cloud Experiment. While the majority of models reproduce the observed structure of a



1 mixed-phase cloud that produces ice precipitation, the median liquid water path of both  
2 SCMs and CRMs is only one-third of the observed value. Thus, there is no evidence that  
3 resolving mesoscale and cloud-scale features in the CRMs improves the simulations  
4 relative to the SCMs for this case. On the other hand, several models have simulated  
5 liquid and ice water paths which are consistent with the observations. Although a general  
6 underestimate of liquid water path in Arctic mixed-phase clouds has been found in  
7 previous studies (Curry et al. 2000, Inoue et al. 2006, Morrison and Pinto 2006, Prenni et  
8 al. 2007, Sandvik et al. 2007), the present study confirms this result in the context of a  
9 highly constrained modeling environment in which identical large-scale advective  
10 tendencies and surface fluxes have been applied to a wide range of model types.

11 There is a trend towards better agreement with the observations of the liquid and ice  
12 water paths as the sophistication of the model microphysics increases from single  
13 moment with T-dependent partitioning to single moment with independent liquid and ice  
14 to double moment. While similar conclusions have been reached in some modeling  
15 studies involving Arctic clouds (Girard and Curry 2001, Morrison and Pinto 2006), this  
16 study involved a wider set of models than these earlier studies. However, also present is a  
17 considerable scatter among the models with a given class of microphysics, so it is unclear  
18 how much significance to give to this trend. More discussion of this issue will be  
19 presented in Part II of this study where a similar trend is also observed.

20 A sensitivity study in which models simulated only a liquid-phase cloud indirectly  
21 suggests that the interaction of ice microphysics with liquid microphysics is responsible

1 for the significant underestimate of liquid water path present in many models. This calls  
2 attention to the widely varying treatment of processes such as ice initiation and the rate at  
3 which ice crystals lower the water vapor beneath that necessary to sustain liquid water in  
4 the clouds (the Bergeron-Findeisen process). This finding is consistent with previous  
5 studies suggesting the importance of ice microphysics in Arctic mixed-phase clouds (e.g.,  
6 Pinto 1998; Harrington et al. 1999; Jiang et al. 2000; Morrison and Pinto 2006; Prenni et  
7 al. 2007). However, there was also significant scatter among the models here in terms of  
8 the relationship between liquid water path and ice crystal concentration, despite strong  
9 sensitivity to crystal concentration found in these previous studies. Our results clearly  
10 show that other factors besides crystal concentration play an important role in producing  
11 differences among the models. A second sensitivity study showed much less dependence  
12 of the simulated liquid and ice water paths on the vertical resolution of the model.

13 Considered as a whole, the results of this study suggest the importance of the treatment of  
14 microphysics in general and ice microphysics in particular in the simulation of Arctic  
15 mixed-phase clouds. However, microphysics is not the sole factor as other factors are  
16 likely to be important. Thus, it is recommended that the GCSS Polar Cloud Working  
17 Group conduct additional studies that further constrain the simulations. One possible  
18 avenue for this work would be to compare different microphysical parameterizations in a  
19 framework where dynamical and radiative processes are fixed and non-interactive with  
20 the simulated cloud microphysics. This may help to resolve some of the unexplained  
21 differences found in the present study and confirm the finding here of overall  
22 improvement of simulations with more detailed microphysical treatments. In particular,

1 the present case is well-suited for the kinematic framework of Morrison and Grabowski  
2 (2007) in which simulations by different microphysical schemes were compared when  
3 they were each subjected to the specified flow corresponding to a single large eddy in a  
4 stratocumulus-topped boundary layer.

5 There may not be a simpler setting for the simulation of mixed-phase clouds.  
6 Complications of multi-layer cloud systems (Curry et al. 1996) or strong feedbacks  
7 between the cloud and the surface temperature and fluxes that happen when mixed-phase  
8 clouds are above sea-ice (Morrison and Pinto 2006) have been eliminated in the present  
9 case. Despite this simplicity, few model simulations are consistent with the observations  
10 reflecting the difficulty of simulating these clouds. The intercomparison of model  
11 simulations of multi-layer clouds observed during M-PACE is presented in Part II of this  
12 study.

13 The relative simplicity of the cloud and its boundary conditions as well as the availability  
14 of high quality observations may make this case study suitable as a benchmark for mixed-  
15 phase clouds. Thin single layer clouds with high amounts of supercooled liquid water that  
16 produce ice precipitation are not limited to the Arctic, but also occur in cold-air outbreaks  
17 at lower latitudes (Kristovich et al. 2000) and middle-level cloud systems (Fleishauer et  
18 al. 2002, Hogan et al. 2003). It is hoped that this case will continue to be an attractive  
19 target for cloud modelers.

20

1 **Acknowledgements.** This work is supported by the Office of Science of the United  
2 States (U. S.) Department of Energy under grants DE-AI02-94ER61768 (DelGenio), DE-  
3 FG02-02ER63370 (Chen), DE-FG02-02ER63337 (McFarquhar), DE-FG02-03ER63539  
4 (Morrison), DE-FG02-05ER63955 (Cole), DE-FG02-05ER63959 (Park), DE-FG02-  
5 05ER64058 (Harrington), DE-FG02-05ER64069 (Wang), DE-AI02-06ER64173  
6 (Ackerman and Fridlind), DE-FG02-06ER64167 (Turner), DE-FG02-06ER64168  
7 (Poellot), DE-FG02-06ER64187 (deBoer), and DE-FG02-07ER64378 (McFarquhar). A.  
8 Ackerman and A. Fridlind are supported by the U. S. National Aeronautics and Space  
9 Administration's (NASA) Radiation Sciences Program and the NASA Advanced  
10 Supercomputing Division. M. Chen is supported by National Science Foundation (NSF)  
11 grant ATM-0415184. J. Cole is supported by the Canadian Foundation for Climate and  
12 Atmospheric Sciences. M. Falk and V. Larson are supported by NSF grant ATM-  
13 0442605 and subaward G-7424-1 from the Department of Defense Center for  
14 Geosciences/Atmospheric Research at Colorado State University via Cooperative  
15 Agreement DAAD19-02-2-0005 with the Army Research Laboratory. C. Hoose is  
16 supported by the climate program of the Swiss National Centre of Competence in  
17 Research. Y. Luo is supported by the Chinese Academy of Meteorological Sciences and  
18 NASA's Cloud Modeling and Analysis Initiative. H. Morrison is supported by NASA  
19 grant NNG06GBB1G and by the NSF Science and Technology Center for Multi-Scale  
20 Modeling of Atmospheric Processes, managed by Colorado State University under  
21 cooperative agreement ATM-0425247. The contribution of S. Klein, R. McCoy, and S.  
22 Xie to this work is performed under the auspices of the U. S. Department of Energy by  
23 Lawrence Livermore National Laboratory under contract DE-AC52-07NA27344. The  
24 Pacific Northwest National Laboratory is operated for the Department of Energy by  
25 Battelle Memorial Institute under contract DE-AC06-76RLO-1830. The National Center  
26 for Atmospheric Research is sponsored by the National Science Foundation. Gratitude is  
27 expressed to Anton Beljaars for providing ECMWF analysis data. The work at Lawrence  
28 Berkeley National Laboratory was supported by the U.S. Department of Energy under  
29 Contract No.DE-AC02-05CH11231.

## 1 **References**

- 2 Ackerman, T. P. and G. Stokes, 2003: The Atmospheric Radiation Measurement  
3 program, *Physics Today*, **56**, 38-45.
- 4 Ackerman, A. S., M. P. Kirkpatrick, D. E. Stevens, and O. B. Toon, 2004: The impact of  
5 humidity above stratiform clouds on indirect aerosol climate forcing. *Nature*, **432**, 1014-  
6 1017, doi:10.1038/nature03174.
- 7 Baumgardner, D. and A. Korolev, 1997: Airspeed corrections for optical array probe  
8 sample volumes. *J. Atmos. Oceanic Tech.*, **14**, 1224–1229.
- 9 Boville, B. A., P. J. Rasch, J. J. Hack, and J. R. McCaa, 2006: Representation of clouds  
10 and precipitation processes in the Community Atmosphere Model Version 3 (CAM3). *J.*  
11 *Clim.*, **19**, 2184–2198.
- 12 Bretherton, C. S. and S. Park, 2008: A new moist turbulence parameterization in the  
13 Community Atmosphere Model. *J. Clim.*, submitted.
- 14 Chen, S. and Coauthors, 2003: COAMPS<sup>®</sup> version 3 model description: General theory  
15 and equations. Navy Research Laboratory Publication #NRL/PU/7500-03-448.
- 16 Collins W. D. and Coauthors, 2006: The formulation and atmospheric simulation of the  
17 Community Atmosphere Model version 3 (CAM3). *J. Clim.*, **19**, 2144–2161.

1 Cotton, W. R. and Coauthors, 2003: RAMS 2001: Current status and future directions.  
2 *Meteor. Atmos. Phys.*, **82**, 5-29.

3 Curry, J. A., W. B. Rossow, D. Randall, and J. L. Schramm, 1996: Overview of Arctic  
4 cloud and radiation characteristics. *J. Clim.*, **9**, 1731-1764.

5 Curry, J. A., J. O. Pinto, T. Benner, and M. Tschudi, 1997: Evolution of the cloudy  
6 boundary layer during the autumnal freezing of the Beaufort Sea, *J. Geophys. Res.*, **102**,  
7 13851–13860.

8 Curry, J. A. and Coauthors, 2000: FIRE Arctic Clouds Experiment. *Bull. Amer. Met.*  
9 *Soc.*, **81**, 5–29.

10 Environmental Modeling Center (EMC), 2003: The GFS atmospheric model. National  
11 Center for Environmental Prediction Office Note 442, U. S. Department of Commerce,  
12 National Oceanic and Atmospheric Administration, 14 pp. Available online at  
13 <http://www.emc.ncep.noaa.gov/officenotes/FullTOC.html>.

14 European Centre for Medium Range Weather Forecasts (ECMWF), 2007: IFS  
15 documentation cycle 31r1. Part IV: Physical processes. 155 pp. Available online at  
16 <http://www.ecmwf.int/research/ifsdocs/CY31r1/index.html>.

17 Ferrier, B., 1994: A double-moment multiple-phase four-class bulk ice scheme. Part I:  
18 Description. *J. Atmos. Sci.*, **51**, 249-280.

1 Field, P. R. and Coauthors, 2004: Simultaneous radar and aircraft observations of  
2 mixed-phase cloud at the 100-m-scale. *Quart. J. Roy. Meteor. Soc.*, **130**, 1877-1904.

3 Flatau, P. J., G. J. Tripoli, J. Verlinde, and W. R. Cotton, 1989: The CSU-RAMS cloud  
4 microphysics module: General theory and code documentation. Colorado State  
5 Department of Atmospheric Science paper no. 451.

6 Fleishauer, R. P., V. E. Larson, and T. H. Vonder Haar, 2002: Observed microphysical  
7 structure of midlevel mixed-phase clouds. *J. Atmos. Sci.*, **59**, 1779-1804.

8 Fridlind, A. M. and Coauthors, 2000: Analysis of gas-aerosol partitioning in the Arctic:  
9 Composition of size-resolved equilibrium model results with field data, *J. Geophys. Res.*,  
10 **105**, 19891-19904.

11 Fridlind, A. M. and Coauthors, 2007: Ice properties of single-layer stratocumulus during  
12 the Mixed-Phase Arctic Cloud Experiment (M-PACE): Part II. Model results. *J.*  
13 *Geophys. Res.*, **112**, D24202, doi:10.1029/2007JD008646.

14 Fu, Q., 1996: An accurate parameterization of the solar radiative properties of cirrus  
15 clouds. *J. Clim.*, **9**, 2058-2082.

16 The GFDL Global Atmospheric Model Development Team (GFDL GAMDT), 2004: The  
17 new GFDL global atmosphere and land model AM2-LM2: Evaluation with prescribed  
18 SST simulations. *J. Clim.*, **17**, 4641-4673.

1 Girard, E. and J. A. Curry, 2001: Simulation of Arctic low-level clouds observed during  
2 the FIRE Arctic Clouds Experiment using a new bulk microphysics scheme, *J. Geophys.*  
3 *Res.*, **106**, 15,139–15,154.

4 Golaz, J.-C., V. E. Larson, and W. R. Cotton, 2002: A PDF-based model for boundary  
5 layer clouds. Part I: Method and model description. *J. Atmos. Sci.*, **59**, 3540-3551.

6 Golaz, J.-C., S. Wang, J. D. Doyle, and J. M. Schmidt, 2005: COAMPS<sup>®</sup>-LES: Model  
7 evaluation and analysis of second and third moment vertical velocity budgets. *Bound.-*  
8 *Layer Meteor.*, **116**, 487-517.

9 Gultepe, I., G. A. Isaac, and S. G. Cober, 2001: Ice crystal number concentration versus  
10 temperature for climate studies. *Int. J. Climatol.*, **21**, 1281-1302.

11 Hansen, J. and Coauthors, 2002: Climate forcings in Goddard Institute for Space Studies  
12 SI2000 simulations. *J. Geophys. Res.*, **107**, 4347, doi:10.1029/2001JD001143.

13 Harrington, J. Y., T. Reisen, W. R. Cotton, and S. M. Kreidenweis, 1999: Cloud  
14 resolving simulations of Arctic stratus. Part II: Transition-season clouds. *Atmos. Res.*, **51**,  
15 45–75.

16 Hashino, T. and G. J. Tripoli, 2007: The spectral ice habitat prediction system (SHIPS).  
17 Part I: Model description and simulation of vapor deposition process. *J. Atmos. Sci.*, **64**,  
18 2210-2237.



- 1 Hobbs, P. V. and A. L. Rangno, 1998: Microstructures of low and middle-level clouds  
2 over the Beaufort sea. *Quart. J. Roy. Meteor. Soc.*, **124**, 2035-2071.
- 3 Hogan, R. J. and Coauthors, 2003: Characteristics of mixed-phase clouds. I: Lidar, radar  
4 and aircraft observations from CLARE'98. *Quart. J. Roy. Meteor. Soc.*, **129**, 2089-2116.
- 5 Iacobellis, S. F. and R. C. J. Somerville, 2006: Evaluating parameterizations of the  
6 autoconversion process using a single-column model and Atmospheric Radiation  
7 Measurement Program measurements. *J. Geophys. Res.*, **111**, D02203,  
8 doi:10.1029/2005JD006296.
- 9 Illingworth, A. J. and Coauthors, 2007: Cloudnet – Continuous evaluation of cloud  
10 profiles in seven operational models using ground-based observations. *Bull. Amer.*  
11 *Meteor. Soc.*, **88**, 883-898.
- 12 Inoue, J., J. Liu, J. O. Pinto, and J. A. Curry, 2006: Intercomparison of Arctic regional  
13 climate models: Modeling clouds and radiation for SHEBA in May 1998. *J. Clim.*, **19**,  
14 4167-4178.
- 15 Intrieri, J. M., M. D. Shupe, T. Uttal, and B. J. McCarty, 2002: An annual cycle of Arctic  
16 cloud characteristics observed by radar and lidar at SHEBA, *J. Geophys. Res.*, **107**, 8030,  
17 doi:10.1029/2000JC000423.

- 1 Jiang, H. and Coauthors, 2000: Cloud resolving simulations of mixed-phase Arctic  
2 stratus observed during BASE: Sensitivity to concentration of ice crystals and large-scale  
3 heat and moisture advection. *J. Atmos. Sci.*, **57**, 2105–2117.
- 4 Key, J. R., and A. J. Schweiger, 1998: Tools for atmospheric radiative transfer: Steamer  
5 and FluxNet. *Computers and Geosciences*, **24**, 443-451.
- 6 Khain, A. P., and I. Sednev, 1996: Simulation of precipitation formation in the Eastern  
7 Mediterranean coastal zone using a spectral microphysics cloud ensemble model. *Atmos.*  
8 *Res.*, **43**, 77-110.
- 9 Khairoutdinov, M. F., and D.A. Randall, 2003: Cloud-resolving modeling of the ARM  
10 summer 1997 IOP: Model formulation, results, uncertainties and sensitivities. *J. Atmos.*  
11 *Sci.*, **60**, 607-625.
- 12 Korolev, A. V. and G. A. Isaac, 2003: Phase transformation in mixed-phase clouds.  
13 *Quart. J. Roy. Meteor. Soc.*, **129**, 19-38.
- 14 Korolev, A. V. and Coauthors, 2003: Observations of the microphysical structure of  
15 mixed-phase clouds. *Quart. J. Roy. Meteor. Soc.*, **129**, 39-66.
- 16 Korolev, A. V. and P. R. Field, 2008: The effect of dynamics on mixed-phase clouds:  
17 Theoretical considerations. *J. Atmos. Sci.*, **65**, 66-86.

- 1 Kristovich, D. A. R. and Coauthors, 2000: The Lake—Induced Convection Experiment  
2 and the snowband dynamics project. *Bull. Amer. Meteor. Soc.*, **81**, 519–542.
- 3 Larson, V. E. and Coauthors, 2006: What determines altocumulus dissipation time? *J.*  
4 *Geophys. Res.*, **111**, D19207, doi:10.1029/2005JD007002.
- 5 Lin, Y.-L., R. Farley, and H. Orville, 1983: Bulk parameterization of the snow field in a  
6 cloud model. *J. Clim. Appl. Met.*, **22**, 1065-1092.
- 7 Liu, X. and J. E. Penner, 2005: Ice nucleation parameterization for global models.  
8 *Meteorologische Zeitschrift*, **22**, 1065-1092.
- 9 Liu, X., J. E. Penner, S. J. Ghan, and M. Wang, 2007a: Inclusion of ice microphysics in  
10 the NCAR Community Atmospheric Model version 3 (CAM3). *J. Clim.*, **20**, 4526-4547.
- 11 Liu X., S. Xie, and S. J. Ghan, 2007b: Evaluation of a new mixed-phase cloud  
12 microphysics parameterization with CAM3 single-column model and M-PACE  
13 observations. *Geophys. Res. Lett.*, **34**, L23712, doi:10.1029/2007GL031446.
- 14 Lohmann, U., P. Stier, C. Hoose, S. Ferrachat, S. Kloster, E. Roeckner, and J. Zhang,  
15 2007: Cloud microphysics and aerosol indirect effects in the global climate model  
16 ECHAM5-HAM. *Atmos. Chem. Phys.*, **7**, 3425-3446.

- 1 Luo, Y., K.-M. Xu, H. Morrison, and G. McFarquhar, 2008a: Arctic mixed-phase  
2 clouds simulated by a cloud-resolving model: Comparison with ARM observations and  
3 sensitivity to microphysics parameterizations. *J. Atmos. Sci.*, **65**, 1285–1303.
- 4 Luo, Y., K.-M. Xu, H. Morrison, G. McFarquhar, Z. Wang, and G. Zhang, 2008b: Arctic  
5 mixed-phase clouds simulated by a cloud-resolving model: Comparison with ARM  
6 observations and sensitivity experiments. *J. Geophys. Res.*, **113**, D12208,  
7 doi:10.1029/2007JD009563.
- 8 Mazin, I. P., 1986: Relation of cloud phase structure to vertical motion. *Sov. Meteor.*  
9 *Hydrol.*, **N11**, 27–35.
- 10 McFarquhar, G. M. and S. G. Cober, 2004: Single-scattering properties of mixed-phase  
11 Arctic clouds at solar wavelengths: Impacts on radiative transfer. *J. Clim.*, **17**, 3799–  
12 3813.
- 13 McFarquhar, G. and Coauthors, 2007a: The importance of small ice crystals to cirrus  
14 properties: Observations from the Tropical Western Pacific International Cloud  
15 Experiment (TWP-ICE). *Geophys. Res. Lett.*, **34**, L13803, doi:10.1029/2007GL029865.
- 16 McFarquhar, G. and Coauthors, 2007b: Ice properties of single layer boundary clouds  
17 during the Mixed-Phase Arctic Cloud Experiment (M-PACE): Part I. Observations. *J.*  
18 *Geophys. Res.*, **112**, D24201, doi:10.1029/2007JD008633.

- 1 Meyers, M. P., P. J. DeMott, and W. R. Cotton, 1992: New primary ice-nucleation  
2 parameterization in an explicit cloud model. *J. Appl. Meteor.*, **31**, 708-721.
- 3 Meyers, M. P., R. L. Walko, J. Y. Harrington, and W. R. Cotton, 1997: New RAMS  
4 cloud microphysics parameterization. Part II: The two-moment scheme. *Atmos. Res.*, **45**,  
5 3-39.
- 6 Morrison, H., M. D. Shupe, and J. A. Curry, 2003: Modeling clouds observed at SHEBA  
7 using a bulk microphysics parameterization implemented into a single-column model. *J.*  
8 *Geophys. Res.*, **108**, 4255, doi:10.1029/2002JD002229.
- 9 Morrison, H., J. A. Curry, and V. I. Khvorostyanov, 2005a: A new double-moment  
10 microphysics parameterization for application in cloud and climate models. Part I:  
11 Description. *J. Atmos. Sci.*, **62**, 1665-1677.
- 12 Morrison, H., J. A. Curry, M. D. Shupe, and P. Zuidema, 2005b: A new double-moment  
13 microphysics parameterization for application in cloud and climate models. Part II:  
14 Single-column modeling of Arctic clouds. *J. Atmos. Sci.*, **62**, 1678-1693.
- 15 Morrison, H. and J. O. Pinto, 2006: Intercomparison of bulk cloud microphysics schemes  
16 in mesoscale simulations of springtime Arctic mixed-phase stratiform clouds. *Mon. Wea.*  
17 *Rev.*, **134**, 1880–1900.
- 18 Morrison, H. and W. W. Grabowski, 2007: Comparison of bulk and bin warm-rain  
19 microphysics models using a kinematic framework. *J. Atmos. Sci.*, **64**, 2839–2861.

- 1 Morrison, H. and A. Gettelman, 2008: A new two-moment stratiform cloud  
2 microphysics parameterization for the Community Atmosphere Model (CAM3). Part I:  
3 Description and numerical tests. *J. Clim.*, **21**, 3642-3659.
- 4 Morrison, H., J. O. Pinto, J. A. Curry, and G. M. McFarquhar, 2008a: Sensitivity of M-  
5 PACE mixed-phase stratocumulus to cloud condensation and ice nuclei over regionally-  
6 varying surface conditions. *J. Geophys. Res.*, **113**, D05203, doi:10.1029/2007JD008729.
- 7 Morrison, H. and Coauthors, 2008b: Intercomparison of model simulations of mixed-  
8 phase clouds observed during the ARM Mixed-Phase Arctic Cloud Experiment. Part II:  
9 Multi-layer cloud. *Quart. J. Roy. Meteor. Soc.*, submitted.
- 10 Neggers, R. A. J., M. Köhler, and A. Beljaars, 2008: A dual mass flux scheme for  
11 boundary layer convection. Part I: Transport. *J. Atmos. Sci.*, submitted.
- 12 Pinto, J. O., 1998: Autumnal mixed-phase cloudy boundary layers in the Arctic. *J. Atmos.*  
13 *Sci.*, **55**, 2016–2038.
- 14 Pinto, J. O., J. A. Curry, and J. M. Intrieri, 2001: Cloud-aerosol interactions during  
15 autumn over Beaufort Sea, *J. Geophys. Res.*, **106**, 15077–15098.
- 16 Prenni, A. J. and Coauthors, 2007: Can ice-nucleating aerosols affect Arctic seasonal  
17 climate? *Bull. Amer. Met. Soc.*, **88**, 541-550.

- 1 Randall, D. A. and Coauthors, 2003: Confronting models with data: The GEWEX Cloud  
2 Systems Study. *Bull. Amer. Met. Soc.*, **84**, 455–469.
- 3 Roeckner, E. and Coauthors, 2003: The atmospheric general circulation model  
4 ECHAM5. Part I: Model description. Report 349, Max Planck Institute for Meteorology,  
5 Hamburg, Germany, available from <http://www.mpimet.mpg.de>.
- 6 Rotstayn, L. D., 1997: A physically based scheme for the treatment of stratiform clouds  
7 and precipitation in large-scale models. I: Description and evaluation of the  
8 microphysical processes. *Quart. J. Roy. Meteor. Soc.*, **123**, 1227-1282.
- 9 Rotstayn, L. D., B. F. Ryan, and J. J. Katzfey, 2000: A scheme for calculation of the  
10 liquid fraction in mixed-phase stratiform clouds in large-scale models. *Mon. Wea. Rev.*,  
11 **128**, 1070–1088.
- 12 Sandvik, A. and Coauthors 2007: Observed and simulated microphysical composition of  
13 Arctic clouds: Data properties and model validation. *J. Geophys. Res.*, **112**,  
14 doi:10.1029/2006JD007351.
- 15 Schmidt, G. A. and Coauthors, 2006: Present day atmospheric simulations using GISS  
16 Model E: Comparison to in-situ, satellite and reanalysis data. *J. Clim.*, **19**, 153-192.
- 17 Shupe, M. D., and J. M. Intrieri, 2004: Cloud radiative forcing of the Arctic surface: The  
18 influence of cloud properties, surface albedo, and solar zenith angle. *J. Clim.*, **17**, 616–  
19 628.

- 1 Shupe, M. D., S. Y. Matrosov, and T. Uttal, 2006: Arctic mixed-phase cloud properties  
2 derived from surface-based sensors at SHEBA. *J. Atmos. Sci.*, **63**, 697–711.
- 3 Shupe, M. D., 2007: A ground-based multiple remote-sensor cloud phase classifier.  
4 *Geophys. Res. Lett.*, **34**, L22809, doi:10.1029/2007GL031008.
- 5 Shupe, M. D., P. Kollias, M. Poellot, and E. Eloranta, 2008: On deriving vertical air  
6 motions from cloud radar Doppler spectra. *J. Atmos. Ocean. Technol.*, **25**, 547–557.
- 7 Shutts, G. J. and M. E. B. Gray, 1994: A numerical modelling study of the geostrophic  
8 adjustment process following deep convection. *Quart. J. Roy. Met. Soc.*, **120**, 1145–1178.
- 9 Stephens, G. L., 1978: Radiation profiles in extended water clouds. II: Parameterization  
10 schemes. *J. Atmos. Sci.*, **35**, 2123–2132.
- 11 Stevens, B. and Coauthors, 2005: Evaluation of large-eddy simulations via observations  
12 of nocturnal marine stratocumulus. *Mon. Wea. Rev.*, **133**, 1443–1462.
- 13 Strapp, J. and Coauthors, 2001: Laboratory measurements of the response of a PMS  
14 OAP-2DC. *J. Atmos. Oceanic Tech.*, **18**, 1150–1170.
- 15 Stull, R. B., 1988: An introduction to boundary layer meteorology. *Kluwer Academic*  
16 *Publishers*, 355 pp.



- 1 Sud, Y. C. and D. Lee, 2007: Parameterization of aerosol indirect effect to complement  
2 McRAS cloud scheme and its evaluation with the 3-year ARM-SGP analyzed data for  
3 single column models. *Atmos. Res.*, accepted.
- 4 Sun, Z. and K. Shine, 1994: Studies of the radiative properties of ice and mixed-phase  
5 clouds. *Quart. J. Roy. Meteor. Soc.*, **120**, 111–137.
- 6 Tripoli, G. J., 1992: A non-hydrostatic mesoscale model designed to simulate scale  
7 interaction. *Mon. Wea. Rev.*, **120**, 1342-1359.
- 8 Turner, D. D., 2005: Arctic mixed-phase cloud properties from AERI-lidar observations:  
9 Algorithm and results from SHEBA. *J. Appl. Meteor.*, **44**, 427-444.
- 10 Turner, D. D. and Coauthors, 2007: Retrieving liquid water path and precipitable water  
11 vapor from Atmospheric Radiation Measurement (ARM) microwave radiometers. *IEEE*  
12 *Trans. Geosci. Remote Sens.*, **45**, 3680-3690, doi:10.1109/TGRS.2007.903703.
- 13 Uttal, T. and Coauthors, 2002: Surface Heat Budget of the Arctic Ocean. *Bull. Amer.*  
14 *Met. Soc.*, **83**, 255–275.
- 15 Verlinde, H. and Coauthors, 2007: The Mixed-Phase Arctic Cloud Experiment (M-  
16 PACE). *Bull. Amer. Met. Soc.*, **88**, 205-221.
- 17 von Salzen, K., 2005: Piecewise log-normal approximation of size distributions for  
18 aerosol modeling. *Atmos. Chem. Phys.*, **5**, 3959-3998.

- 1 Wang, Z. and K. Sassen, 2002: Cirrus cloud microphysical property retrieval using lidar  
2 and radar measurements. Part II: Midlatitude cirrus microphysical and radiative  
3 properties. *J. Atmos. Sci.*, **59**, 2291-2302.
- 4 Wang, Z., 2007: A refined two-channel microwave radiometer liquid water path retrieval  
5 for cold regions by using multiple-sensor measurements, *IEEE Geo. Rem. Sens. Lett.*, **4**,  
6 591-595.
- 7 Wyant, M. C. and Coauthors, 2007: A single-column model intercomparison of a heavily  
8 drizzling stratocumulus-topped boundary layer. *J. Geophys. Res.*, **112**, D24204,  
9 doi:10.1029/2007JD008536.
- 10 Xie, S. and Coauthors, 2002: Intercomparison and evaluation of cumulus  
11 parametrizations under summertime midlatitude continental conditions. *Quart. J. Roy.*  
12 *Meteor. Soc.*, **128**, 1095–1135.
- 13 Xie, S. and Coauthors, 2006: An assessment of the ECMWF model over the Arctic land  
14 using observations from the ARM Mixed-Phase Arctic Cloud Experiment. *J. Geophys.*  
15 *Res.*, **111**, D05107, doi:10.1029/2005JD006509.
- 16 Xie, S. and Coauthors, 2008: Simulations of Arctic Mixed-Phase clouds in forecasts with  
17 CAM3 and AM2 for M-PACE. *J. Geophys. Res.*, **113**, D04211,  
18 doi:10.1029/2007JD009225.

- 1 Xu, K.-M. and S. K. Krueger, 1991: Evaluation of cloudiness parameterizations using a  
2 cumulus ensemble model. A non-hydrostatic mesoscale model designed to simulate scale  
3 interaction. *Mon. Wea. Rev.*, **119**, 342-367.
- 4 Yuan, J., Q. Fu and N. McFarlane, 2006: Tests and improvements of GCM cloud  
5 parameterizations using the CCCMA SCM with the SHEBA data set. *Atmos. Res.*, **82**,  
6 222–238.
- 7 Zhao Q. Y., and F. H. Carr, 1997: A prognostic cloud scheme for operational NWP  
8 models. *Mon. Wea. Rev.*, **125**, 1931–1953.
- 9 Zhu P. and Coauthors, 2005: Intercomparison and interpretation of single-column model  
10 simulations of a nocturnal stratocumulus-topped marine boundary layer. *Mon. Wea. Rev.*,  
11 **133**, 2741-2758.
- 12 Zuidema, P. and Coauthors, 2005: An Arctic springtime mixed-phase cloudy boundary  
13 layer observed during SHEBA. *J. Atmos. Sci.*, **62**, 160–176.

**Table 1**

Characteristics of participating single-column models. For prognostic cloud variables,  $q_l$ ,  $q_i$ ,  $q_r$ ,  $q_s$ , and  $q_g$  are the mixing ratio of cloud liquid, cloud ice, rain, snow and graupel, respectively.  $q_c$  is the mixing ratio of cloud condensate and is equal to the sum of  $q_l$  and  $q_i$ .  $N_l$ ,  $N_i$ ,  $N_r$ ,  $N_s$  and  $N_g$  are the number concentrations of cloud liquid, cloud ice, snow and graupel, respectively. In the table, T, PBL, and std are abbreviations for temperature, planetary boundary layer and standard, respectively. For purposes of this table, the height of the planetary boundary layer is defined as 1350 m.

<i>Model</i>	<i>Investigator and Model reference</i>	<i>Cloud microphysics</i>	<i>Prognostic cloud variables</i>	<i>Do clouds depend on aerosols?</i>	<i># of vertical levels in the PBL at std (high) resolution</i>
ARCSCM	Hugh Morrison <i>Morrison et al. (2003)</i>	double moment <i>Morrison et al. (2005a)</i>	$q_l, q_i, q_r, q_s$ $N_l, N_i, N_r, N_s$	Yes	10 (20)
CCCMA	Jason Cole Knut von Salzen <i>von Salzen (2005)</i>	single moment with independent liquid and ice <i>von Salzen (2005)</i>	$q_l, q_i$	Yes (liquid only)	10 (16)
ECHAM	Corinna Hoose <i>Roeckner et al. (2003)</i>	double moment <i>Lohmann et al. (2007)</i>	$q_l, q_i$ $N_l, N_i$	Yes	6 (23)
ECMWF	Roel Neggers <i>ECMWF (2007)</i>	single moment with T-dependent partitioning (12% liquid at $-15^\circ\text{C}$ ) <i>ECMWF (2007)</i>	$q_c$	No	14
ECMWF-DUALM	Roel Neggers <i>Neggers et al. (2008)</i>	single moment with T-dependent partitioning (12% liquid at $-15^\circ\text{C}$ ) <i>ECMWF (2007)</i>	$q_c$	No	14
GFDL	Stephen Klein <i>GFDL GAMDT (2004)</i>	single moment with independent liquid and ice <i>Rotstajn et al. (2000)</i>	$q_l, q_i$	No	9 (34)
GISS	Audrey Wolf Anthony DelGenio <i>Hansen et al. (2002)</i>	single moment with independent liquid and ice <i>Schmidt et al. (2006)</i>	$q_l, q_i$	No	6

<i>Model</i>	<i>Investigator and Model reference</i>	<i>Cloud microphysics</i>	<i>Prognostic cloud variables</i>	<i>Do clouds depend on aerosols?</i>	<i># of vertical levels in the PBL at std (high) resolution</i>
GISS-LBL	Igor Sednev Surabi Menon <i>Hansen et al. (2002)</i>	bin microphysics <i>Khain and Sednev (1996)</i>	33 bins each for liquid droplets, plates, columns, dendrites, snow, graupel, and frozen drops	Yes	8
MCRAS	Yogesh Sud Gregory Walker <i>Sud and Lee (2007)</i>	single moment with T-dependent partitioning (75% liquid at $-15^{\circ}\text{C}$ ) <i>Sud and Lee (2007)</i>	$q_c, N_i$	Yes (liquid only)	4 (15)
MCRASI	Yogesh Sud Gregory Walker <i>Sud and Lee (2007)</i>	double moment <i>Liu and Penner (2005)</i>	$q_l, q_i$ $N_l, N_i$	Yes	4 (15)
NCEP	Fanglin Yang <i>EMC (2003)</i>	Single moment with T-dependent partitioning (25% liquid at $-15^{\circ}\text{C}$ ) <i>Zhao and Carr (1997)</i>	$q_c$	No	12 (128)
SCAM3	Shaocheng Xie <i>Collins et al. (2006)</i>	single moment with T-dependent partitioning (83% liquid at $-15^{\circ}\text{C}$ ) <i>Boville et al. (2006)</i>	$q_c$	No	4 (14)
SCAM3-LIU	Xiaohong Liu <i>Collins et al. (2006)</i>	double moment <i>Liu et al. (2007a)</i>	$q_l, q_i$ $N_l, N_i$	Yes	4 (14)
SCAM3-MG	Hugh Morrison <i>Collins et al. (2006)</i>	double moment <i>Morrison and Gettelman (2008)</i>	$q_l, q_i$ $N_l, N_i$	Yes	4
SCAM3-UW	Sungsu Park <i>Bretherton and Park (2008)</i>	single moment with T-dependent partitioning (83% liquid at $-15^{\circ}\text{C}$ ) <i>Boville et al. (2006)</i>	$q_c$	No	7 (125)
SCRIPPS	Michael Foster Dana Veron <i>Iacobellis and Somerville (2006)</i>	single moment with independent liquid and ice <i>Rotstayn (1997)</i>	$q_l, q_i$	No	7 (17)
UWM	Michael Falk Vincent Larson <i>Golaz et al. (2002)</i>	single moment with independent liquid and ice <i>Larson et al. (2006)</i>	$q_l, q_i$	No	51 (146)

**Table 2**

As in Table 1 but for participating cloud-resolving models. The dimensionality of the model is listed as two-dimensional (2D) or three-dimensional (3D).  $q_p$  is the mixing ratio of precipitating condensate and is equal to the sum of  $q_r$ ,  $q_s$ , and  $q_g$ .

<i>Model</i>	<i>Investigator and Model reference</i>	<i>Cloud microphysics</i>	<i>Prognostic cloud variables</i>	<i>Do clouds depend on aerosols ?</i>	<i>Dimensionality, Horizontal (std vertical) resolution, Domain size</i>	<i># of vertical levels in the PBL at std (high) resolution</i>
COAMPS <sup>®</sup>	Jean-Christophe Golaz Jerome Schmidt <i>Golaz et al. (2005)</i>	double moment <i>Chen et al. (2003)</i>	$q_l, q_i, q_r, q_s, q_g$ $N_l, N_i, N_r$	No	3D 50m (20m) 4.8km by 4.8km	67
DHARMA	Ann Fridlind Andy Ackerman <i>Ackerman et al. (2004)</i>	bin microphysics <i>Fridlind et al. (2007)</i>	20 liquid, 20 ice, and 40 dissolved solute bins	Yes	3D 50m (21m) 3.2km by 3.2km	64
METO	Ben Shipway <i>Shutts and Gray (1994)</i>	double moment <i>Ferrier (1994)</i>	$q_l, q_i, q_r, q_s, q_g$ $N_l, N_s, N_g$	No	3D 50m (50m) 6.4km by 6.4km	27 (53)
NMS-BULK	Gijs deBoer Tempei Hashino <i>Tripoli (1992)</i>	double moment <i>Flatau et al. (1989)</i>	$q_l, q_i, q_r, q_s, q_g$ $N_l, N_i, N_r, N_s,$ $N_g$	No	2D 200m (100m) 60 km	13
NMS-SHIPS	Gijs deBoer Tempei Hashino <i>Tripoli (1992)</i>	bin microphysics <i>Hashino and Tripoli (2007)</i>	21 liquid, 20 ice and 1 aerosol bins	Yes (ice only)	2D 200m (100m) 60km	13
RAMS-CSU	Alex Avramov Jerry Harrington <i>Cotton et al. (2003)</i>	double moment <i>Meyers et al. (1997)</i>	$q_l, q_i, q_r, q_s, q_g$ $N_l, N_i, N_s, N_g$	Yes (ice only)	2D 1000m (70m) 150km	17 (29)
SAM	Mingxuan Chen Marat Khairoutdinov <i>Khairoutdinov and Randall (2003)</i>	single moment with T-dependent partitioning (25% liquid at $-15^\circ\text{C}$ ) <i>Khairoutdinov and Randall (2003)</i>	$q_c, q_p$	No	3D 100m (50m) 12.7km by 12.7km	27 (53)
UCLA-LARC	Yali Luo Kuan-Man Xu <i>Luo et al. (2008a)</i>	double moment <i>Morrison et al. (2005a)</i>	$q_l, q_i, q_r, q_s$ $N_l, N_i, N_r, N_s$	Yes	2D 2km (180m) 256km	7 (23)
UCLA-LARC-LIN	Yali Luo Kuan-Man Xu <i>Xu and Krueger (1991)</i>	single moment with independent liquid and ice <i>Lin et al. (1983)</i>	$q_l, q_i, q_r, q_s, q_g$	No	2D 2km (180m) 256 km	7 (23)

**Table 3**

Median condensate water paths and inter-quartile ranges in parentheses from observations for the study period.

	Liquid water path ( $\text{g m}^{-2}$ )	Ice water path ( $\text{g m}^{-2}$ )
<i>Aircraft</i>		
Flight 1009	130.1 (94.2-143.2)	8.0 (4.7-16.4)
Flight 1010a	109.3 (101.2-116.9)	3.5 (2.5-11.7)
Combined flights	115.3 (98.3-135.7)	7.6 (3.4-14.7)
<i>Ground-based</i>		
SHUPE-TURNER @ Barrow	224.2 (172.3-280.8)	30.7 (19.2-42.8)
WANG @ Barrow	195.6 (141.2-251.3)	28.1 (22.3-38.0)
TURNER @ Oliktok Point	87.6 (69.1-103.5)	
WANG @ Oliktok Point	127.9 (102.0-151.6)	

**Table 4**

Median condensate water paths from models for simulation hours four through twelve. Results are reported for the standard experiment as well as sensitivity experiments in which ice microphysics are disabled and higher vertical resolution employed. Where available, the rain, snow, graupel water paths are included the reported total liquid and ice water paths. Asterisks (\*) indicate SCMs for which the rain and snow water paths were unavailable. Median SCM ice water paths are computed using only models which report snow water paths.

	Liquid water path ( $\text{g m}^{-2}$ )			Ice water path ( $\text{g m}^{-2}$ )	
	Standard	No ice	High Resolution	Standard	High Resolution
Median model	56.7	208.0	63.1	25.9	26.0
Median SCM	56.0	256.2	64.4	29.1	35.9
Median CRM	57.3	183.6	63.1	17.1	22.8
Median model with single moment with T-dependent partitioning microphysics	21.2	258.6	21.7	33.8	35.9
Median model with single moment with independent liquid and ice microphysics	72.8	263.1	63.1	31.8	28.8
Median model with double moment microphysics	100.0	183.6	195.7	19.9	10.3
Median model	69.1			17.0	



	Liquid water path ( $\text{g m}^{-2}$ )			Ice water path ( $\text{g m}^{-2}$ )	
with bin microphysics					
<i>SCMs</i>					
ARCSCM	291.8	358.6	306.0	11.8	9.9
CCCMA	264.9	269.9	336.5	11.5	1.2
ECHAM*	165.5	164.4	239.8	1.0	2.5
ECMWF	5.8			55.9	
ECMWF-DUALM	21.2			171.2	
GFDL	51.0	278.8	35.0	29.2	27.6
GISS*	47.8			20.8	
GISS-LBL	29.8	187.8		26.0	
MCRAS*	13.7	309.1	8.7	2.6	1.2
MCRASI*	20.1	577.8	8.9	2.7	11.3
NCEP*	16.1	60.6	21.7	39.6	56.6
SCAM3	172.9		233.6	28.8	35.9
SCAM3-LIU	144.5		40.0	31.1	131.5
SCAM3-MG	56.0			24.0	
SCAM3-UW	172.9	208.0	126.5	29.1	62.2
SCRIPPS*	112.0	140.4	49.0	13.5	12.3
UWM	88.2	256.2	79.8	37.0	36.0
<i>CRMs</i>					
COAMPS <sup>®</sup>	24.1	267.3		25.7	
DHARMA	135.7	217.8		17.0	
METO	29.7	77.6	36.7	22.7	24.3
NMS-BULK	1.6	82.0		17.1	
NMS-SHIPS	69.1	65.2		0.03	
RAMS-CSU	172.6	172.8	222.4	0.007	0.014
SAM	23.3	328.5	20.2	33.8	22.8
UCLA-LARC	167.5	194.4	195.7	8.4	10.3
UCLA-LARC-LIN	57.3		63.1	34.4	30.0

## Figure captions

Figure 1. Moderate resolution imaging spectroradiometer composite visible image of the North slope of Alaska and Beaufort Sea for October 9, 2004. The boundary layer clouds occurred when cold air above the sea ice to the northeast of Alaska flowed over the ice-free Beaufort Sea inducing the significant surface heat fluxes responsible for cloud formation. The sea ice is visible in the upper right corner of the image. The clouds were observed in the northeasterly flow between the ARM stations of Barrow and Oliktok Point on the coast of snow-covered Alaska. As is common in “cold-air outbreak” stratocumulus, boundary layer “rolls” or “cloud streets” developed with a horizontal scale that increases in the downstream direction.

Figure 2. Initial conditions for model simulations of the potential temperature (right panel, thick line) and mixing ratios of water vapor (left panel, thick line) and cloud liquid (left panel, dashed line). Also shown are the values of the potential temperature (right panel, thin line) and water vapor mixing ratio (left panel, thin line) from the 17Z 9 October 2004 sounding at Barrow. The triangle in the right panel indicates the value of the ocean surface potential temperature in the coastal region.

Figure 3. Vertical pressure velocity ( $\Omega$ ) and the horizontal advective tendencies of temperature and water vapor mixing ratio for the period 17Z 9 October to 5Z 10 October 2004. Each panel displays the values from the ECMWF analysis (solid line) and the values used in the model simulations (dots).

Figure 4. Time-averaged cloud fraction from observations and models as a function of height. The observations panel depicts the fraction of time at each height that cloud was observed from remote sensors at Barrow (SHUPE-TURNER) and the two aircraft flights during the period 17Z 9 October to 5Z 10 October 2004. Model panels depict statistical properties of the mean cloud fraction for hours four through twelve of model simulations. The properties depicted include the median of models (solid black line), the inner 50% of models (dark shading), and the outer 50% of models (light shading).

Figure 5. Time averaged hydrometeor fraction from models and the remote sensors at Barrow (SHUPE-TURNER, dashed line).

Figure 6. Time-averaged fraction of observations with a given phase as a function of normalized height. Phase categories include liquid-phase only, ice-phase only, and mixed-phase. Normalized height is defined such that 0 is cloud base, 1 is cloud top, and -1 is the surface. The remote sensor retrievals are from SHUPE-TURNER.

Figure 7. Scatterplot of the median liquid water path and ice water path from observations (letters) and model simulations (symbols). The aircraft observations are depicted by the letter “A”, whereas the remote sensing retrievals of SHUPE-TURNER and WANG are depicted by the letters “S” and “W”, respectively. The lightly dashed rectangle indicates the likely range of the regionally averaged liquid and ice water path. The filling or lack thereof in a symbol indicates the model type and the symbol shape indicates the class of model cloud microphysics. See the legend in the plot for the key. As observations do not distinguish between precipitating and non-precipitating condensate,

the reported water paths include the contributions from the precipitating species. SCMs for which the precipitation species were unavailable are indicated with a “\*” in the center of the symbol. One model falls outside the plot domain and is depicted with a “↑” attached to its symbol which points to the numerical value of the ordinate. A 1:1 line is plotted for reference.

Figure 8. Liquid water content from models and aircraft data as a function of normalized height. Each panel depicts the statistical properties of the profiles including the median value, and the inner and outer 50% of the data as in Figure 4. For the aircraft data, the statistical properties are computed from the high-frequency data. For the models, the statistical properties are computed from the set of model median profile values.

Figure 9. As in Figure 8 but for ice water content. The remote sensing retrievals are from WANG. Note that there are no aircraft data at normalized heights less than  $-0.6$ . The SCM plot is constructed by only using the models which report snow water paths.

Figure 10. Scatterplot the median ice crystal number concentration and liquid water path from aircraft observations (depicted by the letter “A”) and model simulations (symbols). Ice crystal number concentrations are weighted by ice water content and averaged over profiles for the aircraft data and time and height for the models. Symbols are plotted with the same convention as in Figure 7.

Figure 11. The vertical profiles of total water mixing ratio ratio  $q_t$  and ice-liquid water potential temperature  $\theta_{li}$  from the models. Each panel depicts the statistical properties

(median, inner and outer 50%) of the model median profiles as well as the values from the initial condition.

Figure 12. Scatterplot of solar transmission and total condensate water path. Solar transmission is computed as the average downward component to the broadband solar radiation at the surface divided by the average insolation at the top-of-the-atmosphere. Model results are indicated with symbols with the same convention as in Figure 7. The observations from the radiation measurements and remote sensing retrievals at Barrow are indicated by OBS. The results of STREAMER radiation calculations performed with an ice-free ocean or snow-covered land surface are indicated by S-O and S-L, respectively.

Figure 13. As in Figure 12 but for the downward longwave radiative flux at the surface.

Figure 14. Scatterplot of the model simulated liquid water path from a sensitivity study in which ice microphysics were disabled and the total (liquid + ice) condensate water path from the control simulation. A 1:1 line is shown.

Figure 15. Scatterplot of the ratio of the total condensate water path in the no-ice sensitivity study to that of the control simulation and the fraction of the total condensate water path in the control simulation that is in the ice-phase. Note that the y-axis is logarithmic and that two models fall outside the plot domain.

Figure 16. Scatterplot of the model simulated total (liquid + ice) condensate water path from a sensitivity study in which models used increased vertical resolution and the control simulations.



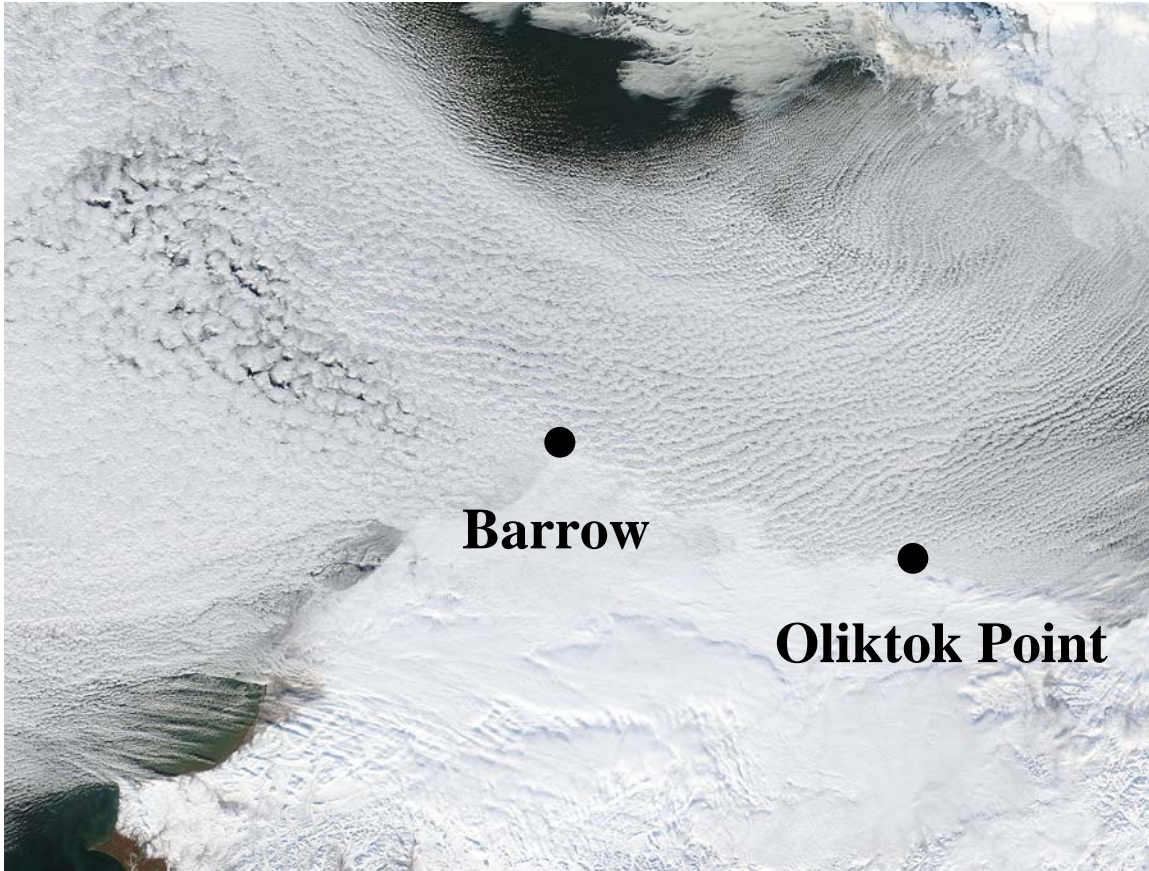


Figure 1. Moderate resolution imaging spectroradiometer composite visible image of the North slope of Alaska and Beaufort Sea for October 9, 2004. The boundary layer clouds occurred when cold air above the sea ice to the northeast of Alaska flowed over the ice-free Beaufort Sea inducing the significant surface heat fluxes responsible for cloud formation. The sea ice is visible in the upper right corner of the image. The clouds were observed in the northeasterly flow between the ARM stations of Barrow and Oliktok Point on the coast of snow-covered Alaska. As is common in “cold-air outbreak” stratocumulus, boundary layer “rolls” or “cloud streets” developed with a horizontal scale that increases in the downstream direction.

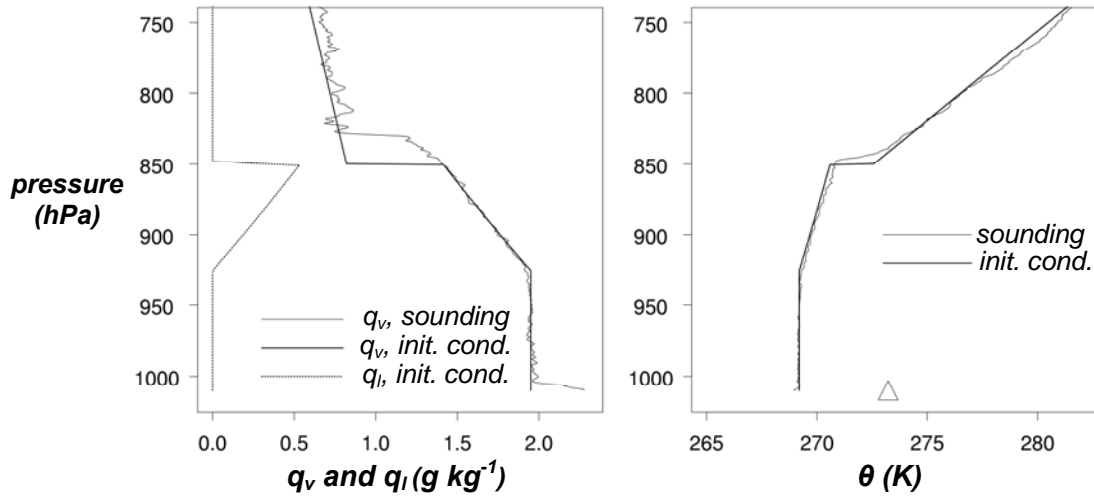


Figure 2. Initial conditions for model simulations of the potential temperature (right panel, thick line) and mixing ratios of water vapor (left panel, thick line) and cloud liquid (left panel, dashed line). Also shown are the values of the potential temperature (right panel, thin line) and water vapor mixing ratio (left panel, thin line) from the 17Z 9 October 2004 sounding at Barrow. The triangle in the right panel indicates the value of the ocean surface potential temperature in the coastal region.



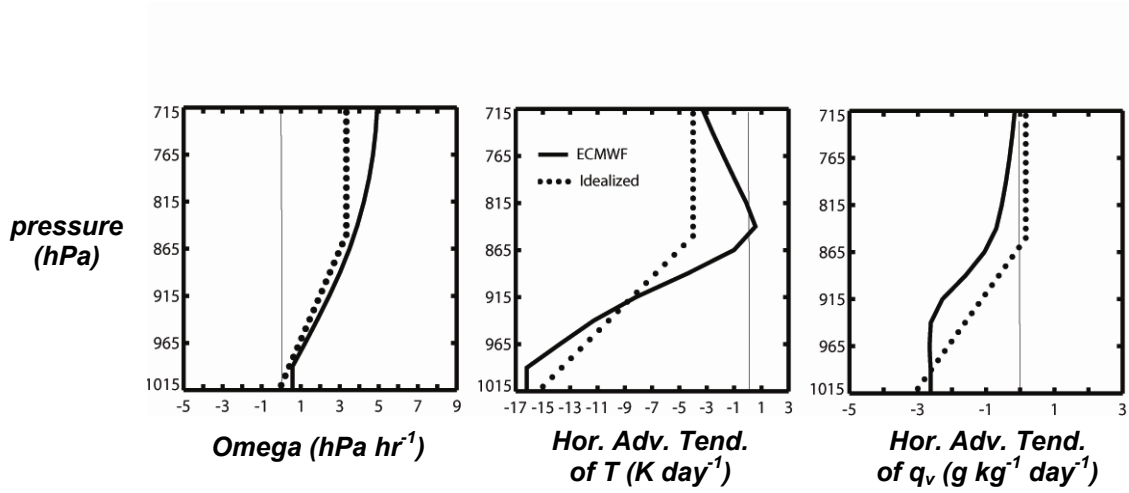


Figure 3. Vertical pressure velocity ( $\Omega$ ) and the horizontal advective tendencies of temperature and water vapor mixing ratio for the period 17Z 9 October to 5Z 10 October 2004. Each panel displays the values from the ECMWF analysis (solid line) and the values used in the model simulations (dots).

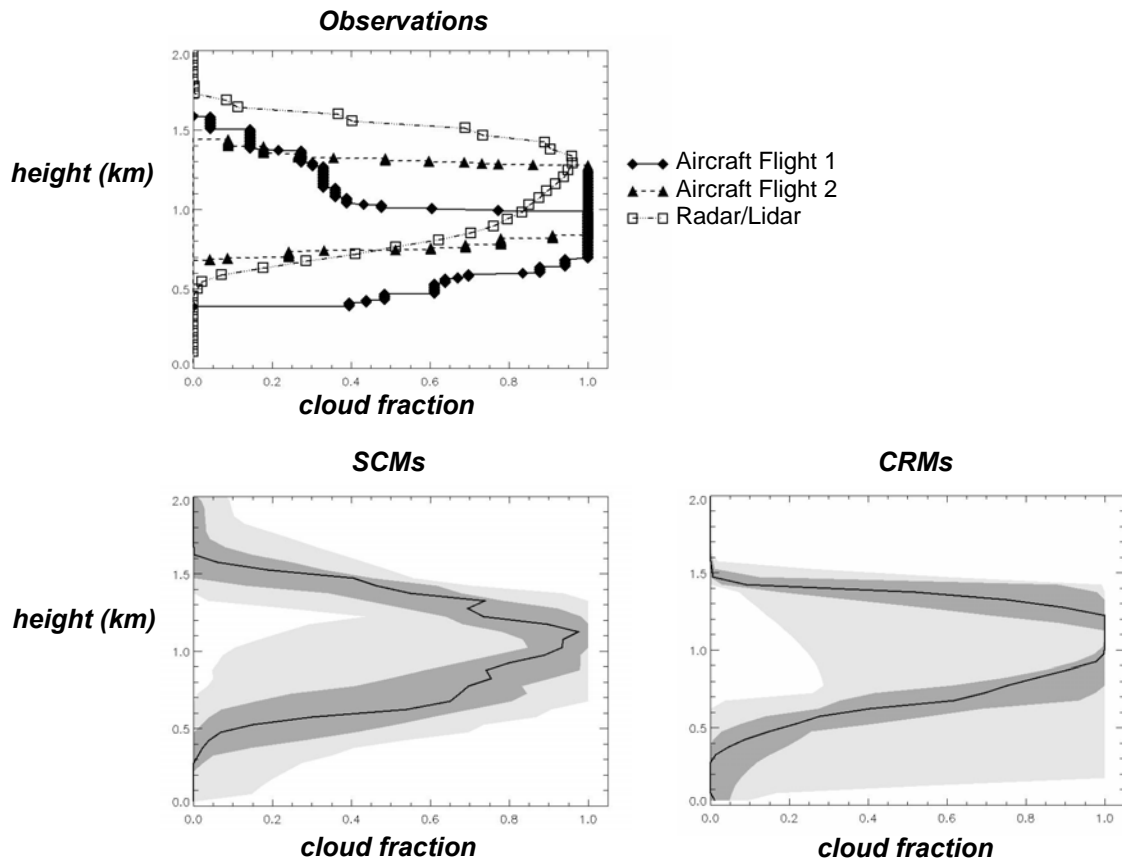


Figure 4. Time-averaged cloud fraction from observations and models as a function of height. The observations panel depicts the fraction of time at each height that cloud was observed from remote sensors at Barrow (SHUPE-TURNER) and the two aircraft flights during the period 17Z 9 October to 5Z 10 October 2004. Model panels depict statistical properties of the mean cloud fraction for hours four through twelve of model simulations. The properties depicted include the median of models (solid black line), the inner 50% of models (dark shading), and the outer 50% of models (light shading).

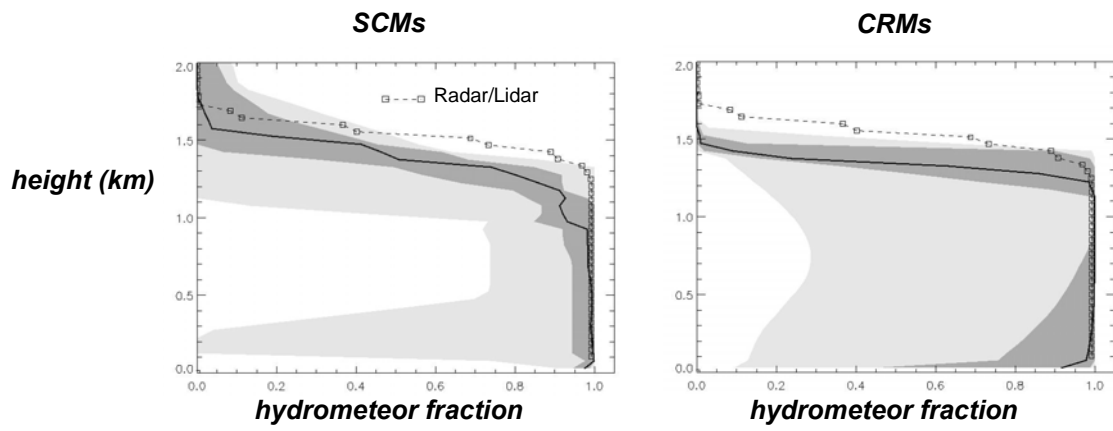


Figure 5. Time averaged hydrometeor fraction from models and the remote sensors at Barrow (SHUPE-TURNER, dashed line).

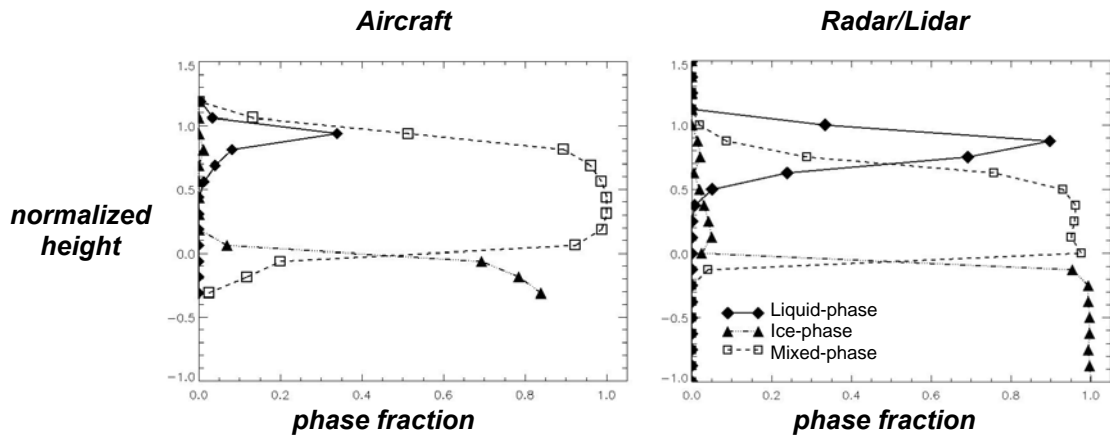


Figure 6. Time-averaged fraction of observations with a given phase as a function of normalized height. Phase categories include liquid-phase only, ice-phase only, and mixed-phase. Normalized height is defined such that 0 is cloud base, 1 is cloud top, and  $-1$  is the surface. The remote sensor retrievals are from SHUPE-TURNER.

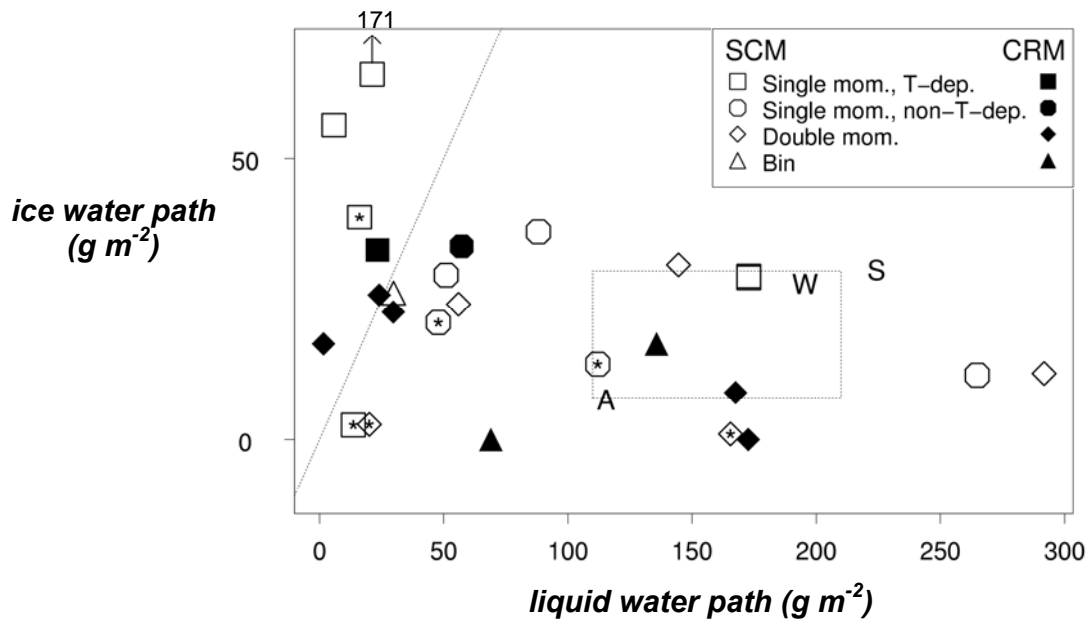


Figure 7. Scatterplot of the median liquid water path and ice water path from observations (letters) and model simulations (symbols). The aircraft observations are depicted by the letter “A”, whereas the remote sensing retrievals of SHUPE-TURNER and WANG are depicted by the letters “S” and “W”, respectively. The lightly dashed rectangle indicates the likely range of the regionally averaged liquid and ice water path. The filling or lack thereof in a symbol indicates the model type and the symbol shape indicates the class of model cloud microphysics. See the legend in the plot for the key. As observations do not distinguish between precipitating and non-precipitating condensate, the reported water paths include the contributions from the precipitating species. SCMs for which the precipitation species were unavailable are indicated with a “\*” in the center of the symbol. One model falls outside the plot domain and is depicted with a “↑” attached to its symbol which points to the numerical value of the ordinate. A 1:1 line is plotted for reference.

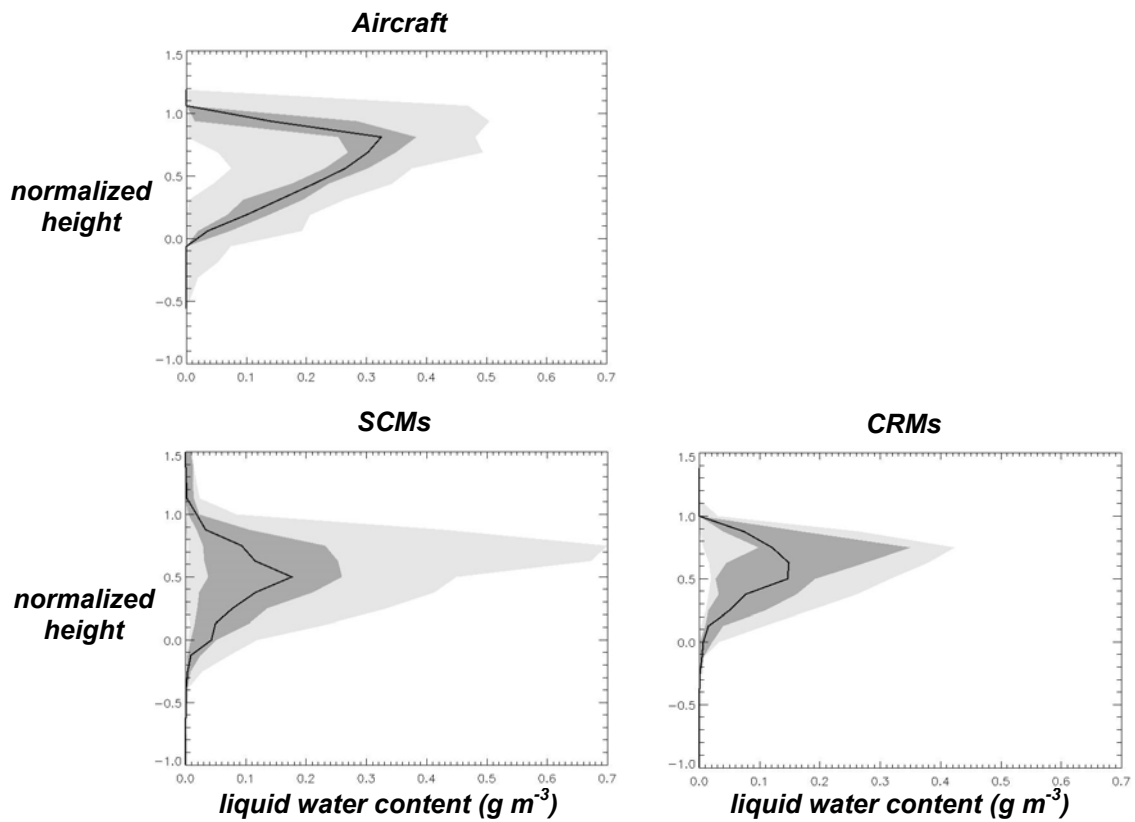


Figure 8. Liquid water content from models and aircraft data as a function of normalized height. Each panel depicts the statistical properties of the profiles including the median value, and the inner and outer 50% of the data as in Figure 4. For the aircraft data, the statistical properties are computed from the high-frequency data. For the models, the statistical properties are computed from the set of model median profile values.

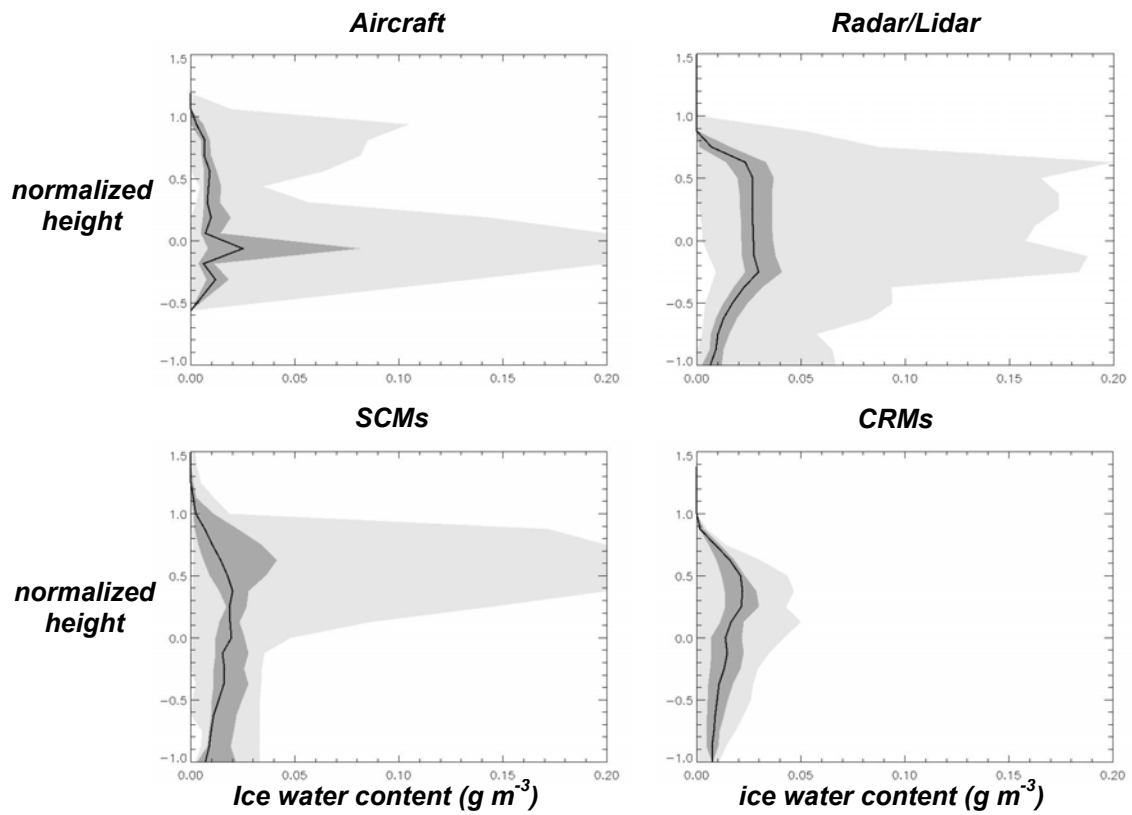


Figure 9. As in Figure 8 but for ice water content. The remote sensing retrievals are from WANG. Note that there are no aircraft data at normalized heights less than  $-0.6$ . The SCM plot is constructed by only using the models which report snow water paths.

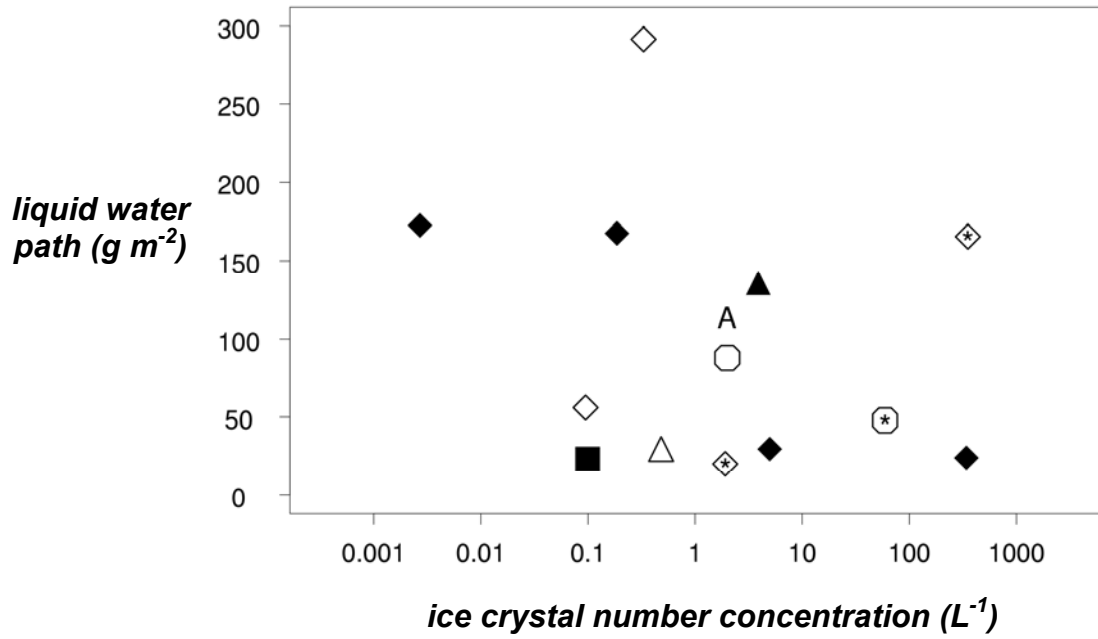


Figure 10. Scatterplot the median ice crystal number concentration and liquid water path from aircraft observations (depicted by the letter “A”) and model simulations (symbols). Ice crystal number concentrations are weighted by ice water content and averaged over profiles for the aircraft data and time and height for the models. Symbols are plotted with the same convention as in Figure 7.



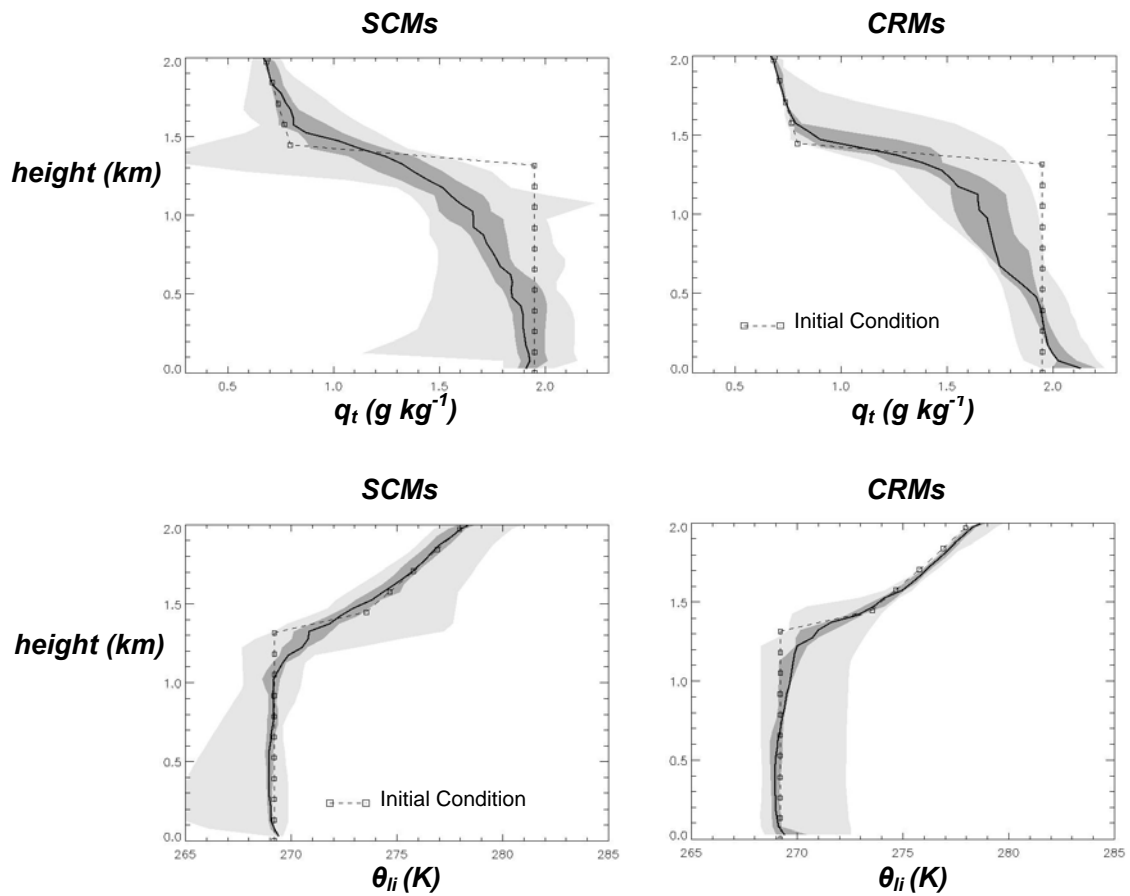


Figure 11. The vertical profiles of total water mixing ratio  $q_t$  and ice-liquid water potential temperature  $\theta_{li}$  from the models. Each panel depicts the statistical properties (median, inner and outer 50%) of the model median profiles as well as the values from the initial condition.

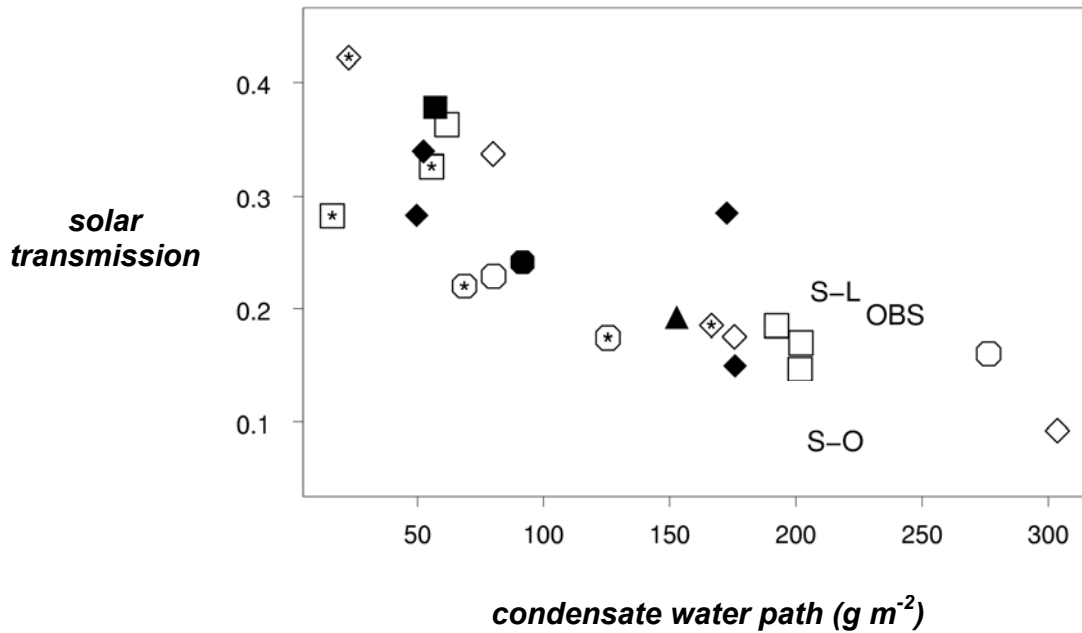


Figure 12. Scatterplot of solar transmission and total condensate water path. Solar transmission is computed as the average downward component to the broadband solar radiation at the surface divided by the average insolation at the top-of-the-atmosphere. Model results are indicated with symbols with the same convention as in Figure 7. The observations from the radiation measurements and remote sensing retrievals at Barrow are indicated by OBS. The results of STREAMER radiation calculations performed with an ice-free ocean or snow-covered land surface are indicated by S-O and S-L, respectively.

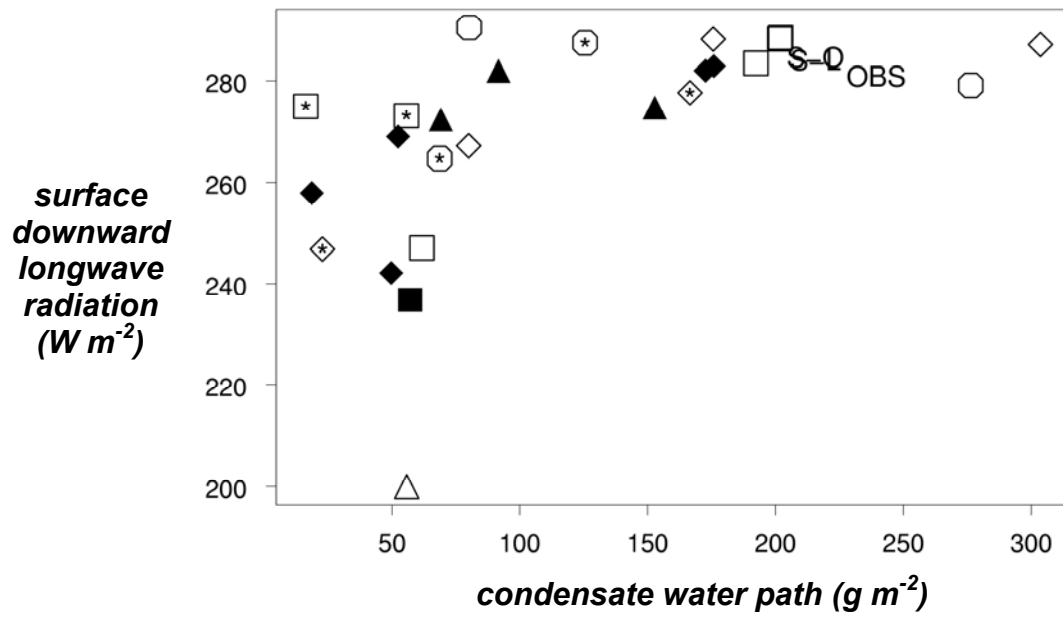


Figure 13. As in Figure 12 but for the downward longwave radiative flux at the surface.

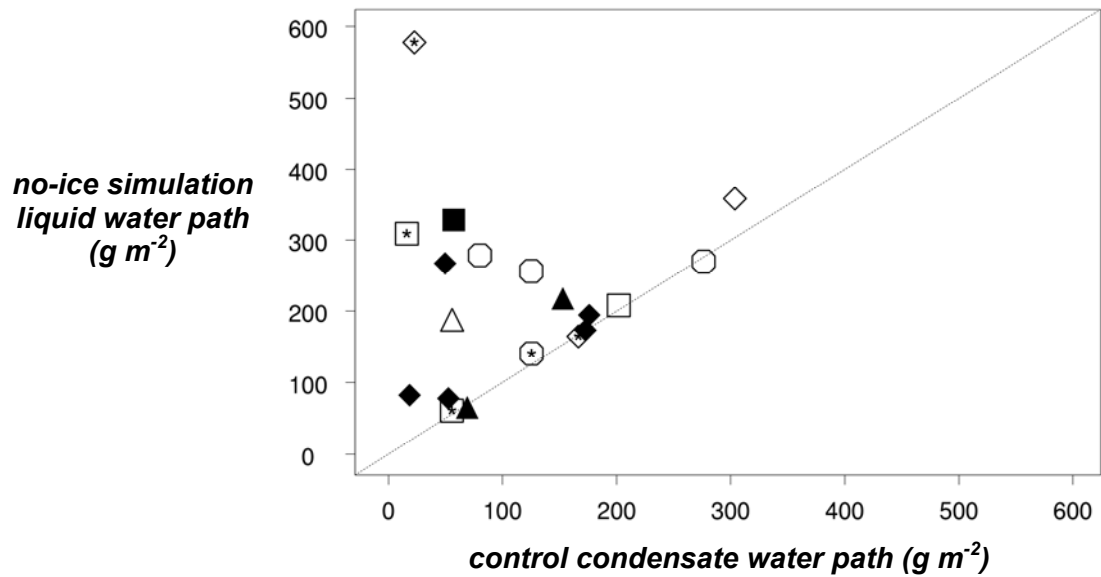


Figure 14. Scatterplot of the model simulated liquid water path from a sensitivity study in which ice microphysics were disabled and the total (liquid + ice) condensate water path from the control simulation. A 1:1 line is shown.

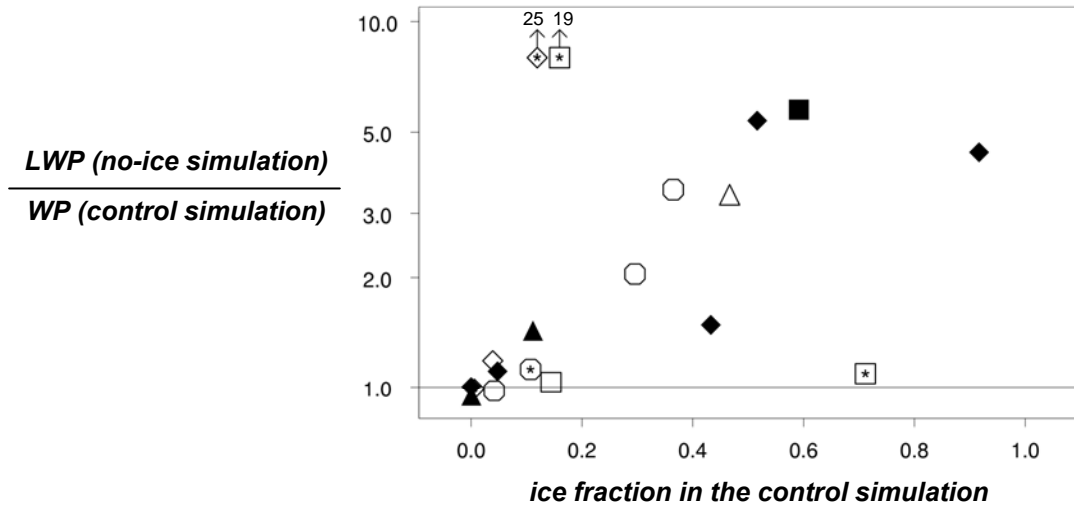


Figure 15. Scatterplot of the ratio of the total condensate water path in the no-ice sensitivity study to that of the control simulation and the fraction of the total condensate water path in the control simulation that is in the ice-phase. Note that the y-axis is logarithmic and that two models fall outside the plot domain.

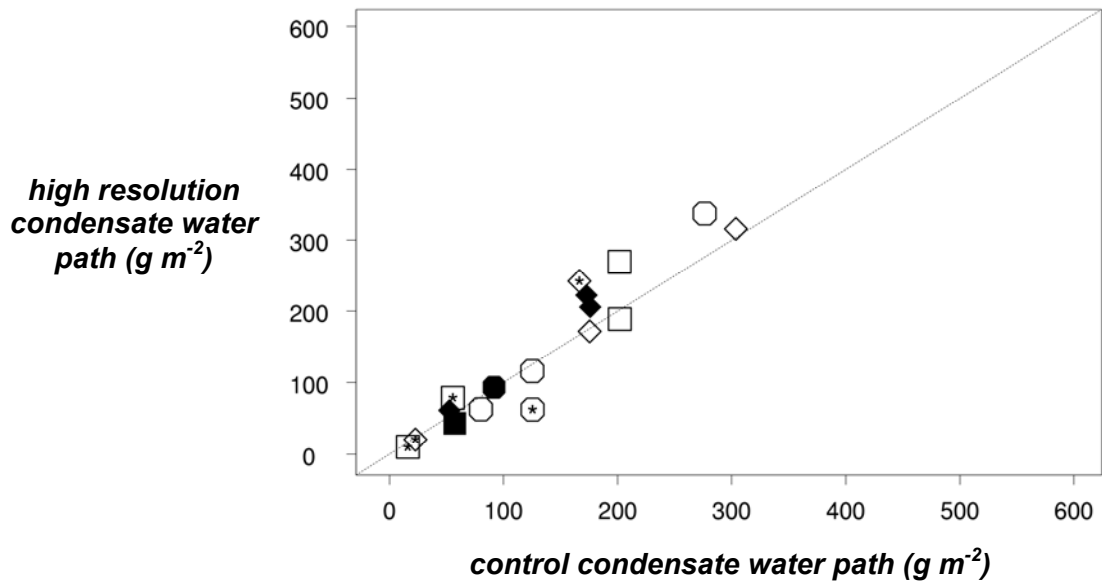


Figure 16. Scatterplot of the model simulated total (liquid + ice) condensate water path from a sensitivity study in which models used increased vertical resolution and the control simulation.